Two-temperature Navier-Stokes equations for a polyatomic gas derived from kinetic theory

Two-temperature Navier–Stokes equations for a polyatomic gas derived from kinetic theory

Kazuo Aoki[1], Marzia Bisi[2], Maria Groppi[2], and Shingo Kosuge[3]
[1] *Department of Mathematics, National Cheng Kung University, Tainan 70101, Taiwan*
[2] *Department of Mathematical, Physical and Computer Sciences, University of Parma, 43124 Parma, Italy and*
[3] *Institute for Liberal Arts and Sciences, Kyoto University, Kyoto 606-8501, Japan*
(Dated: July 16, 2020)

A polyatomic gas with slow relaxation of the internal modes is considered, and the Navier–Stokes equations with two temperatures, the translational and internal temperatures, are derived for such a gas on the basis of the ellipsoidal-statistical (ES) model of the Boltzmann equation for a polyatomic gas, proposed by Andries *et al.* [P. Andries *et al.*, Eur. J. Mech. B/Fluids **19**, 813 (2000)], by the Chapman–Enskog procedure. Then, the derived equations are applied to numerically investigate the structure of a plane shock wave in CO_2 gas, which is known to have slowly relaxing internal modes. The results show good agreement with those obtained by the direct numerical analysis of the ES model for moderately strong shock waves. In particular, the results perfectly reproduce the double-layer structure of the shock profiles consisting of a thin front layer with rapid change and a thick rear layer with slow relaxation of the internal modes.

I. INTRODUCTION

Polyatomic gas flows play important roles in various applications in high-temperature gas dynamics, such as the entry of space vehicles into earth or planet atmosphere. Since the gas is in highly non-equilibrium in most of applications, the treatment based on kinetic theory, i.e., the Boltzmann equation, is required. However, for a polyatomic gas, the Boltzmann equation, which takes the molecular structure into account, becomes much more complex than that for a monatomic gas [1–7]. Therefore, it is a formidable task to apply the Boltzmann equation itself to practical flow problems. To bypass this difficulty, either simplified kinetic model equations of the Boltzmann equation [8–19], such as those of the Bhatnagar–Gross–Krook (BGK) type, or macroscopic equations of fluid dynamics type [4, 6, 20–25] are often employed.

Many kinetic models for a polytomic gas have been proposed since 1960s [8–19], even in the presence of simple chemical reactions [26, 27]. Most of the kinetic models are constructed in such a way that some fundamental and global properties of the original Boltzmann equation are satisfied, the details of collision mechanics not being considered. Since they are much more tractable than the original Boltzmann equation, they have been playing crucial roles in practical applications.

Nevertheless, the kinetic models are more computationally demanding than the fluid dynamic or macroscopic equations. Therefore, there have been various attempts to construct macroscopic equations on the basis of kinetic or purely macroscopic considerations [4, 6, 17, 20–25]. One of the standard approaches is to derive equations of Euler and Navier–Stokes types using the Chapman–Enskog procedure [4, 6, 20, 25] from the Boltzmann equation. In the case of a polyatomic gas, the standard Chapman–Enskog expansion [28] leads to the ordinary Navier–Stokes equations with bulk viscosity. However, depending on the structure of a polyatomic molecule, there are significant differences in characteristic (or relaxation) times of different internal modes. It is known that, in such a case, the ordinary Navier–Stokes equations are not sufficient to describe flow properties [20, 23, 25].

To overcome this difficulty, some authors have introduced the Euler- or Navier–Stokes-type equations with multi temperatures associated with the translational motion and the internal modes of a molecule [20, 25], starting from the Boltzmann equation. For this purpose, one has to use either (i) an assumption on the magnitude of the relaxation times of the internal modes [20] or (ii) the detailed properties of rotational and individual vibrational modes of a molecule of a specific gas, such as carbon dioxide (CO_2) [25]. The approach (i) is general. However, because of its formal and abstract setting, its application to practical flow problems is not straightforward and rather difficult. The approach (ii) is precise. However, it requires a large amount of information on the molecular structure, containing numerical and empirical formulas and some assumptions, for individual gases.

In the present study, we will propose a set of macroscopic equations of Navier–Stokes type with two temperatures, which we will call the *two-temperature* Navier–Stokes equations (or system). Unlike the previous studies [20, 25], our starting point is not the original Boltzmann equation but the polyatomic version of the ellipsoidal-statistical (ES) model, which is one of the widely used kinetic models proposed in [13] and re-derived in a systematic way in [29]. The model contains a parameter that is related to the bulk viscosity in the ordinary Navier–Stokes equations with one temperature, as well as to the speed of relaxation of the internal modes. Under the assumption that this parameter is as small as the Knudsen number, we carry out the Chapman–Enskog expansion [28] to derive the two-temperature Navier–Stokes equations. Since the number of parameters contained in the ES model is much less than the original Boltzmann equation, the transport properties of the resulting two-temperature Navier–Stokes system in terms of the parameters are much simpler and perfectly explicit. Therefore, it has a wide applicability to practical flow problems. In fact, we will apply the system to the problem of the structure of a stationary shock wave in CO_2 gas and demonstrate that it gives good agreement with the numerical solution based on the ES model [30, 31].

It should be mentioned that some authors have developed macroscopic equations with multi temperatures, other than the Navier–Stokes type, for a polyatomic gas on the basis of the rational extended thermodynamics [17, 21–24]. The moment equations of the Boltzmann equation or its model equations are considered, and appropriate moment-closure assumptions are introduced using the entropy principle. They have been applied to the shock-structure problem successfully, and interesting results have been reported for CO_2 gas [32–35]. In fact, these results motivated the study based on kinetic theory in [18, 30, 31].

We should also give a brief remark on the direct simulation Monte Carlo (DSMC) method [36], which is a powerful numerical method for the Boltzmann equation. This method has been widely used also for diatomic and polytomic gases. In this case, however, because of the lack of information about collision processes, we need phenomenological assumptions on the transition probabilities [37] or database constructed by detailed molecular dynamics simulations for a specific gas [38]. The latter approach is accurate and interesting, but the construction of the database is difficult for polyatomic gases.

The present paper is organized as follows. After this introduction, the ES model and its basic properties are summarized in Sec. II. Then, with an appropriate setting of parameters, the two-temperature Navier–Stokes system is derived by the Chapman–Enskog method in Sec. III. In Sec. IV, the derived system is applied to the problem of the structure of a stationary plane shock wave in CO_2 gas, and it is shown that its numerical solution gives good agreement with the numerical solution based on the ES model. Section V is devoted to brief remarks.

II. ES MODEL AND ITS BASIC PROPERTIES

In the present section, we summarize the ES model for a polyatomic gas that was proposed in [13] and re-derived in a systematic way in [29] and its basic and related properties.

A. ES model

Let us consider a polyatomic gas and denote by δ the number of the internal degrees of freedom of the gas molecule, where δ is a constant such that $\delta \geq 2$. Then, the specific heat at constant volume c_v, that at constant pressure c_p, and the ratio of the specific heats $\gamma = c_p/c_v$ are all constant and are expressed as

$$c_v = \frac{\delta+3}{2}R, \qquad c_p = \frac{\delta+5}{2}R, \qquad \gamma = \frac{\delta+5}{\delta+3}. \tag{1}$$

Here, R is the gas constant per unit mass and is related to the Boltzmann constant k_{B} and the mass of a molecule m by $R = k_{\mathrm{B}}/m$.

Let t be the time variable, $\boldsymbol{X}$ (or X_i) the position vector in the physical space, and $\boldsymbol{\xi}$ (or ξ_i) the molecular velocity. In addition, let $\mathcal{E}$ be the energy per unit mass associated with the internal modes (i.e., the combined energy for the δ modes), which is continuous ranging from 0 to ∞. We denote the number of the gas molecules, at time t, contained in an infinitesimal

volume $d\boldsymbol{X}d\boldsymbol{\xi}d\mathcal{E}$ around a point $(\boldsymbol{X}, \boldsymbol{\xi}, \mathcal{E})$ in the seven-dimensional (extended) phase space consisting of $\boldsymbol{X}$, $\boldsymbol{\xi}$, and $\mathcal{E}$ by

$$\frac{1}{m} f(t, \boldsymbol{X}, \boldsymbol{\xi}, \mathcal{E}) d\boldsymbol{X} d\boldsymbol{\xi} d\mathcal{E}. \tag{2}$$

Therefore, $f(t, \boldsymbol{X}, \boldsymbol{\xi}, \mathcal{E})$ is the mass density in the seven-dimensional phase space. We call $f(t, \boldsymbol{X}, \boldsymbol{\xi}, \mathcal{E})$ the velocity-energy distribution function of the gas molecules. It is governed by the ES model of the Boltzmann equation for a polyatomic gas [13, 29], which can be written in the following form:

$$\frac{\partial f}{\partial t} + \xi_i \frac{\partial f}{\partial X_i} = Q(f), \tag{3}$$

where

$$Q(f) = A_c(T)\rho(\mathcal{G} - f), \tag{4a}$$

$$\mathcal{G} = \frac{\rho \mathcal{E}^{\delta/2-1}}{(2\pi)^{3/2}(\det \mathsf{T})^{1/2}(RT_{\rm rel})^{\delta/2}\Gamma(\delta/2)} \times \exp\left(-\frac{1}{2}(\mathsf{T}^{-1})_{ij}(\xi_i - v_i)(\xi_j - v_j) - \frac{\mathcal{E}}{RT_{\rm rel}}\right), \tag{4b}$$

$$(\mathsf{T})_{ij} = (1-\theta)[(1-\nu)RT_{\rm tr}\delta_{ij} + \nu p_{ij}/\rho] + \theta RT\delta_{ij}, \tag{4c}$$

$$\rho = \iint_0^\infty f d\mathcal{E} d\boldsymbol{\xi}, \tag{4d}$$

$$v_i = \frac{1}{\rho}\iint_0^\infty \xi_i f d\mathcal{E} d\boldsymbol{\xi}, \tag{4e}$$

$$p_{ij} = \iint_0^\infty (\xi_i - v_i)(\xi_j - v_j) f d\mathcal{E} d\boldsymbol{\xi}, \tag{4f}$$

$$T_{\rm tr} = \frac{1}{3R\rho}\iint_0^\infty |\boldsymbol{\xi} - \boldsymbol{v}|^2 f d\mathcal{E} d\boldsymbol{\xi}, \tag{4g}$$

$$T_{\rm int} = \frac{2}{\delta R\rho}\iint_0^\infty \mathcal{E} f d\mathcal{E} d\boldsymbol{\xi}, \tag{4h}$$

$$T = \frac{3T_{\rm tr} + \delta T_{\rm int}}{3+\delta}, \tag{4i}$$

$$T_{\rm rel} = \theta T + (1-\theta)T_{\rm int}. \tag{4j}$$

Here, ρ is the density, $\boldsymbol{v}$ (or v_i) the flow velocity, p_{ij} the stress tensor, $T_{\rm tr}$ the temperature associated with the translational energy, $T_{\rm int}$ the temperature associated with the energy of the internal modes, T the temperature, $d\boldsymbol{\xi} = d\xi_1 d\xi_2 d\xi_3$, and the domain of integration with respect to $\boldsymbol{\xi}$ is its whole space $\mathbb{R}^3$. The symbol δ_{ij} indicates the Kronecker delta, and $\nu \in [-1/2, 1)$ and $\theta \in (0, 1]$ are the constants that adjust the Prandtl number and the bulk viscosity. In addition, $A_c(T)$ is a function of T such that $A_c(T)\rho$ is the collision frequency of the gas molecules, $\Gamma(z)$ is the gamma function defined by

$$\Gamma(z) = \int_0^\infty s^{z-1}e^{-s} ds, \tag{5}$$

T is the 3×3 matrix with its (i,j) component defined by Eq. (4c), and $\det\mathsf{T}$ and T^{-1} are, respectively, its determinant and inverse. Here and in what follows, we basically use the summation convention, i.e., $a_i b_i = \sum_{i=1}^3 a_i b_i$, $a_i^2 = \sum_{i=1}^3 a_i^2$, $a_i b_j c_{ij} = \sum_{i,j=1}^3 a_i b_j c_{ij}$, etc.

The other important macroscopic quantities, the pressure p and the heat-flow vector q_i, are defined by

$$p = R\rho T, \tag{6}$$

$$q_i = \iint_0^\infty (\xi_i - v_i)\left(\frac{1}{2}|\boldsymbol{\xi} - \boldsymbol{v}|^2 + \mathcal{E}\right) f d\mathcal{E} d\boldsymbol{\xi}, \tag{7}$$

where Eq. (6) is the equation of state.

It should be noted that in Ref. [13], the variable I, which is related to our $\mathcal{E}$ as $\mathcal{E} = I^{2/\delta}$, is used as an independent variable instead of $\mathcal{E}$. See Ref. [39] or Appendix A in Ref. [40] for the relation between the notation in Ref. [13] and that of the present paper (see also [19]). In the ES model (3), the energy associated with the internal modes is expressed by a single continuous variable $\mathcal{E}$. Some models also use a continuous energy variable (e.g., [10, 14, 19]), whereas the others use a discrete energy variable (e.g., [8, 9, 11, 12]). However, the corresponding macroscopic equations are analogous in both cases (see, e.g., [16]). Concerning the structure of Eq. (3), one might, for instance, think that it is more natural to use $T_{\rm tr}$, instead of T, in Eqs. (4c) and (4j). If $T_{\rm tr}$ is used, however, the conservation of energy and the entropy inequality in Sec. II B are not satisfied.

B. Basic properties

The ES model (3) has the basic properties listed in the following.

Equilibrium: The vanishing of the collision term $Q(f) = 0$ is equivalent to the fact that f is the following local equilibrium distribution [13] (see also Appendix A in [31]):

$$f_{\rm eq} = \frac{\rho \mathcal{E}^{\delta/2-1}}{(2\pi RT)^{3/2}(RT)^{\delta/2}\Gamma(\delta/2)} \exp\left(-\frac{|\boldsymbol{\xi} - \boldsymbol{v}|^2}{2RT} - \frac{\mathcal{E}}{RT}\right), \tag{8}$$

where ρ, $\boldsymbol{v}$, and T are arbitrary functions of t and $\boldsymbol{X}$.

Conservation: For an arbitrary function $g(t, \boldsymbol{X}, \boldsymbol{\xi}, \mathcal{E})$, the following relation holds [13] (see also Appendix A in [31]):

$$\iint_0^\infty \varphi_r Q(g) d\mathcal{E} d\boldsymbol{\xi} = 0, \tag{9}$$

where φ_r ($r = 0, ..., 4$) are the so-called collision invariants, i.e.,

$$\varphi_0 = 1, \qquad \varphi_i = \xi_i \quad (i = 1, 2, 3), \qquad \varphi_4 = \frac{1}{2}|\boldsymbol{\xi}|^2 + \mathcal{E}. \tag{10}$$

Entropy inequality: For an arbitrary function $g(t, \boldsymbol{X}, \boldsymbol{\xi}, \mathcal{E})$, the following inequality holds [13]:

$$\iint_0^\infty \left(\ln \frac{g}{\mathcal{E}^{\delta/2-1}}\right) Q(g) d\mathcal{E} d\boldsymbol{\xi} \le 0, \tag{11}$$

and the equality sign holds if and only if $g = f_{\rm eq}$ in Eq. (8).

Mean free path: The mean free path l_0 of the gas molecules in the equilibrium state at rest at density ρ_0 and temperature T_0 is given by

$$l_0 = \frac{2}{\sqrt{\pi}} \frac{(2RT_0)^{1/2}}{A_c(T_0)\rho_0}, \tag{12}$$

for Eq. (3), since $A_c(T_0)\rho_0$ is the collision frequency at this equilibrium state.

C. Bulk viscosity and parameter θ

When the mean free path of the gas molecules l_0 is small compared with the characteristic length of the system, we can formally derive the ordinary (compressible) Navier–Stokes equations for a polyatomic gas from the ES model (3) by the Chapman–Enskog method [13]. The Navier–Stokes constitutive laws thus obtained are as follows (see Sec. VI of [41] for these forms and for the entire Navier–Stokes equations):

$$p_{ij} = p\delta_{ij} - \mu(T)\left(\frac{\partial v_i}{\partial X_j} + \frac{\partial v_j}{\partial X_i} - \frac{2}{3}\frac{\partial v_k}{\partial X_k}\delta_{ij}\right) - \mu_b(T)\frac{\partial v_k}{\partial X_k}\delta_{ij}, \tag{13a}$$

$$q_i = -\lambda(T)\frac{\partial T}{\partial X_i}, \tag{13b}$$

where $\mu(T)$, $\mu_b(T)$, and $\lambda(T)$ are, respectively, the viscosity, the bulk viscosity, and the thermal conductivity and are expressed as follows:

$$\mu(T) = \frac{1}{1-\nu+\theta\nu}\frac{RT}{A_c(T)}, \tag{14a}$$

$$\mu_b(T) = \frac{2}{3}\frac{\delta}{\theta(\delta+3)}\frac{RT}{A_c(T)}, \tag{14b}$$

$$\lambda(T) = \frac{\delta+5}{2}\frac{R^2T}{A_c(T)}. \tag{14c}$$

From Eqs. (14a), (14c), and (1), the Prandtl number $\mathrm{Pr} = c_p\mu/\lambda$ is obtained as

$$\mathrm{Pr} = 1/(1-\nu+\theta\nu), \tag{15}$$

and from Eqs. (14a), (14b), (15), and (1), the ratio μ_b/μ is expressed as

$$\frac{\mu_b}{\mu} = \frac{2}{3}\frac{\delta}{\theta(\delta+3)}\frac{1}{\mathrm{Pr}} = \frac{1}{\theta}\left(\frac{5}{3}-\gamma\right)\frac{1}{\mathrm{Pr}}. \tag{16}$$

Here, it should be noted that the ratio μ_b/μ does not depend on T and is inversely proportional to the parameter θ contained in the ES model.

D. Relaxation of internal modes and parameter θ

In this section, we examine the speed of relaxation of the internal modes. For this purpose, we consider the space homogeneous case, where f does not depend on $\boldsymbol{X}$, i.e., $f = f(t, \boldsymbol{\xi}, \mathcal{E})$. Then, the ES model (3) reduces to

$$\frac{\partial f}{\partial t} = A_c(T)\rho(\mathcal{G} - f). \tag{17}$$

If we integrate Eq. (17) and that multiplied by $\boldsymbol{\xi}$, respectively, over the whole space of $\boldsymbol{\xi}$ and whole range of $\mathcal{E}$ and take into account Eqs. (4d), (4e), and (9), we have

$$\frac{d\rho}{dt} = 0, \qquad \frac{d(\rho\boldsymbol{v})}{dt} = 0, \tag{18}$$

that is, ρ and $\boldsymbol{v}$ are constants. Next, we multiply Eq. (17) by $|\boldsymbol{\xi}-\boldsymbol{v}|^2$ and $\mathcal{E}$, respectively, and integrate over the whole ranges of $\boldsymbol{\xi}$ and $\mathcal{E}$. Considering the fact that ρ and $\boldsymbol{v}$ are constants and making use of Eqs. (4g) and (4h) and the moments of $\mathcal{G}$ calculated in Appendix A in [31], we obtain

$$\frac{dT_{\mathrm{tr}}}{dt} = \theta A_c(T)\rho\left(T - T_{\mathrm{tr}}\right), \tag{19a}$$

$$\frac{dT_{\mathrm{int}}}{dt} = \theta A_c(T)\rho\left(T - T_{\mathrm{int}}\right). \tag{19b}$$

It is readily seen from Eqs. (4i) and (19) that

$$\frac{dT}{dt} = 0, \tag{20}$$

i.e., T is a constant.

Let $T_{\rm tr}$ and $T_{\rm int}$ at the initial time $t = 0$ be $T_{\rm tr*}$ and $T_{\rm int*}$, respectively, where $T_{\rm tr*}$ and $T_{\rm int*}$ need to satisfy $(3T_{\rm tr*} + \delta T_{\rm int*})/(3 + \delta) = T$. Then, Eq. (19) gives the following solutions:

$$T_{\rm tr} = T + (T_{\rm tr*} - T)\, e^{-\theta A_c(T)\rho t}, \tag{21a}$$

$$T_{\rm int} = T + (T_{\rm int*} - T)\, e^{-\theta A_c(T)\rho t}. \tag{21b}$$

These solutions indicate that the temperature $T_{\rm int}$ associated with the energy of the internal modes, as well as the temperature $T_{\rm tr}$ associated with the translational energy, approaches the total temperature T with the time scale $1/[\theta A_c(T)\rho]$. Since $A_c(T)\rho$ is the collision frequency of the gas molecules, $1/[A_c(T)\rho]$ is the mean free time. Therefore, we can say that the time scale of relaxation of the internal modes is (mean free time)$/\theta$. This means that small values of θ correspond to slow relaxation of the internal modes.

In the case of the original Boltzmann equation, when the phenomenon under consideration contains two different time scales, the collision term is naturally split into two collision terms with different collision frequencies [20]. On the other hand, the ES model (3) seemingly contains only one time scale, i.e., the mean free time $1/[A_c(T)\rho]$. However, as can be seen from Eq. (21), it has an additional *hidden* time scale $1/\theta$ that controls the speed of relaxation of the internal modes.

E. Remarks and strategy

Some gases are known to have large bulk viscosity. For instance, according to p. 30 in [42], the ratio μ_b/μ of the bulk viscosity to the viscosity and the Prandtl number Pr are $(\mu_b/\mu, \text{Pr}) = (32, 0.71)$ for H_2 gas and (1000, 0.75) for CO_2 gas at 300 K and 1 atm. Therefore, if we set $\delta = 2$ for H_2 gas (thus $\gamma = 7/5$) and $\delta = 4$ for CO_2 gas (thus $\gamma = 9/7$), then from Eq. (16) we obtain $\theta = 0.0117$ for H_2 gas and 5.08×10^{-4} for CO_2 gas. In this way, large values of μ_b/μ lead to small values of θ.

It is a common understanding that the large bulk viscosity is related to the slow relaxation of the internal modes [43, 44]. As we have seen in Secs. II C and II D, the ES model gives a consistent result, that is, both the large bulk viscosity and the large relaxation time lead to small values of θ. The reader is referred to [44] concerning gases with large bulk viscosity other than H_2 and CO_2. The impact of large bulk viscosity for H_2 gas flows is investigated in [45]. Here, it should be mentioned that some authors are doubtful about the large values of μ_b/μ for CO_2 gas [25, 46]. However, in the present study, we follow the view that μ_b/μ is large for CO_2 gas.

If the values of μ_b/μ, Pr, and δ (or γ) are known for a gas, the parameters ν and θ contained in the ES model are determined from Eqs. (15) and (16). Here, it should be noted that the viscosity μ and the bulk viscosity μ_b make sense under the assumption of the Navier–Stokes stress tensor, Eq. (13a). More specifically, if the shear and normal stresses are measured for known velocity, pressure, and temperature fields, μ and μ_b are determined on the basis of Eq. (13a). As long as Eq. (13a) is assumed, large μ_b/μ gives small θ. However, for the ES model (3), Eq. (13a) is derived by the Chapman–Enskog expansion for small Knudsen numbers under the implicit assumption that the parameter θ is of the order of unity. If θ is small ($\theta \ll 1$), therefore, the validity of the Navier–Stokes equations based on Eq. (13) is questionable. In other words, we should take into account the smallness of θ explicitly in order to derive the appropriate fluid-dynamic equations. Therefore, in the present study, we assume that θ is small and of the same order of magnitude as the Knudsen number and try to derive the correct fluid-dynamic equations for small θ, i.e., for a gas with large μ_b/μ or slow relaxation of the internal modes, from the ES model (3) by the Chapman–Enskog procedure.

III. TWO-TEMPERATURE NAVIER–STOKES EQUATIONS

In this section, we will derive the two-temperature Navier–Stokes system, under the assumption that the parameter θ contained in the ES model (3) is as small as the Knudsen number.

A. Non-dimensionalization

In this subsection, we non-dimensionalize the ES model introducing appropriate dimensionless variables. Let L be the reference length, t_0 the reference time, and $p_0 = R\rho_0 T_0$ the reference pressure, where ρ_0 and T_0 are the reference density and temperature. We further choose t_0 as

$$t_0 = L/(2RT_0)^{1/2}. \tag{22}$$

This corresponds to the so-called fluid-dynamic scaling in time. Let us introduce the dimensionless quantities ($\hat{t}$, x_i, ζ_i, $\hat{\mathcal{E}}$, $\hat{f}$, $\hat{\mathcal{G}}$, $\hat{\rho}$, $\hat{v}_i$, $\hat{T}_{\rm tr}$, $\hat{T}_{\rm int}$, $\hat{T}$, $\hat{T}_{\rm rel}$, $\hat{p}_{ij}$, $\hat{p}$, $\hat{q}_i$, $\hat{A}_c(\hat{T})$), which correspond to the original dimensional quantities (t, X_i, ξ_i, $\mathcal{E}$, f, $\mathcal{G}$, ρ, v_i, $T_{\rm tr}$, $T_{\rm int}$, T, $T_{\rm rel}$, p_{ij}, p, q_i, $A_c(T)$), by the following relations:

$$\begin{aligned}
&\hat{t} = t/t_0, \quad x_i = X_i/L, \quad \zeta_i = \xi_i/(2RT_0)^{1/2}, \quad \hat{\mathcal{E}} = \mathcal{E}/RT_0, \\
&(\hat{f}, \hat{\mathcal{G}}) = (f, \mathcal{G})/2\rho_0(2RT_0)^{-5/2}, \quad \hat{\rho} = \rho/\rho_0, \quad \hat{v}_i = v_i/(2RT_0)^{1/2}, \\
&(\hat{T}_{\rm tr}, \hat{T}_{\rm int}, \hat{T}, \hat{T}_{\rm rel}) = (T_{\rm tr}, T_{\rm int}, T, T_{\rm rel})/T_0, \quad \hat{p}_{ij} = p_{ij}/p_0, \quad \hat{p} = p/p_0, \\
&\hat{q}_i = q_i/p_0(2RT_0)^{1/2}, \quad \hat{A}_c(\hat{T}) = A_c(T)/A_c(T_0).
\end{aligned} \tag{23}$$

We occasionally use the bold-faced letters $\boldsymbol{x}$, $\boldsymbol{\zeta}$, $\hat{\boldsymbol{v}}$, and $\hat{\boldsymbol{q}}$ in place of x_i, ζ_i, $\hat{v}_i$, and $\hat{q}_i$, respectively.

Then, the dimensionless version of the ES model (3) is obtained in the following form:

$$\frac{\partial \hat{f}}{\partial \hat{t}} + \zeta_i \frac{\partial \hat{f}}{\partial x_i} = \frac{1}{\epsilon}\hat{Q}(\hat{f}), \tag{24}$$

where

$$\hat{Q}(\hat{f}) = \hat{A}_c(\hat{T})\hat{\rho}(\hat{\mathcal{G}} - \hat{f}), \tag{25a}$$

$$\hat{\mathcal{G}} = \frac{\hat{\rho}\hat{\mathcal{E}}^{\delta/2-1}}{\pi^{3/2}(\det\hat{\mathsf{T}})^{1/2}\,\hat{T}_{\rm rel}^{\delta/2}\Gamma(\delta/2)} \times \exp\left(-(\hat{\mathsf{T}}^{-1})_{ij}(\zeta_i - \hat{v}_i)(\zeta_j - \hat{v}_j) - \frac{\hat{\mathcal{E}}}{\hat{T}_{\rm rel}}\right), \tag{25b}$$

$$(\hat{\mathsf{T}})_{ij} = (1-\theta)[(1-\nu)\hat{T}_{\rm tr}\delta_{ij} + \nu\hat{p}_{ij}/\hat{\rho}] + \theta\hat{T}\delta_{ij}, \tag{25c}$$

$$\hat{\rho} = \iint_0^\infty \hat{f} d\hat{\mathcal{E}} d\boldsymbol{\zeta}, \tag{25d}$$

$$\hat{v}_i = \frac{1}{\hat{\rho}}\iint_0^\infty \zeta_i \hat{f} d\hat{\mathcal{E}} d\boldsymbol{\zeta}, \tag{25e}$$

$$\hat{p}_{ij} = 2\iint_0^\infty (\zeta_i - \hat{v}_i)(\zeta_j - \hat{v}_j)\hat{f} d\hat{\mathcal{E}} d\boldsymbol{\zeta}, \tag{25f}$$

$$\hat{T}_{\rm tr} = \frac{2}{3\hat{\rho}}\iint_0^\infty (\zeta_k - \hat{v}_k)^2 \hat{f} d\hat{\mathcal{E}} d\boldsymbol{\zeta}, \tag{25g}$$

$$\hat{T}_{\rm int} = \frac{2}{\delta\hat{\rho}}\iint_0^\infty \hat{\mathcal{E}}\hat{f} d\hat{\mathcal{E}} d\boldsymbol{\zeta}, \tag{25h}$$

$$\hat{T} = \frac{3\hat{T}_{\rm tr} + \delta\hat{T}_{\rm int}}{3+\delta}, \tag{25i}$$

$$\hat{T}_{\rm rel} = \theta\hat{T} + (1-\theta)\hat{T}_{\rm int}. \tag{25j}$$

Here, ϵ is a quantity of the order of the Knudsen number Kn defined by

$$\epsilon = \frac{\sqrt{\pi}}{2}{\rm Kn} = \frac{\sqrt{\pi}}{2}\frac{l_0}{L}, \tag{26}$$

$d\boldsymbol{\zeta} = d\zeta_1 d\zeta_2 d\zeta_3$, and the domain of integration with respect to $\boldsymbol{\zeta}$ is its whole space $\mathbb{R}^3$. The (dimensionless) pressure $\hat{p}$ and heat-flow vector $\hat{q}_i$ are given by

$$\hat{p} = \hat{\rho}\hat{T}, \tag{27}$$

and

$$\hat{q}_i = \hat{q}_{({\rm tr})i} + \hat{q}_{({\rm int})i}, \tag{28a}$$

$$\hat{q}_{({\rm tr})i} = \iint_0^\infty (\zeta_i - \hat{v}_i)|\boldsymbol{\zeta} - \hat{\boldsymbol{v}}|^2 \hat{f} d\hat{\mathcal{E}} d\boldsymbol{\zeta}, \tag{28b}$$

$$\hat{q}_{({\rm int})i} = \iint_0^\infty (\zeta_i - \hat{v}_i)\hat{\mathcal{E}}\hat{f} d\hat{\mathcal{E}} d\boldsymbol{\zeta}. \tag{28c}$$

The dimensionless form of the basic properties of the ES model given in Sec. II B are summarized in the following.

Equilibrium: $\hat{Q}(\hat{f}) = 0$ is equivalent to the fact that $\hat{f}$ is the dimensionless local equilibrium given by

$$\hat{f}_{\rm eq} = \frac{\hat{\rho}\hat{\mathcal{E}}^{\delta/2-1}}{(\pi\hat{T})^{3/2}\hat{T}^{\delta/2}\Gamma(\delta/2)} \exp\left(-\frac{|\boldsymbol{\zeta} - \hat{\boldsymbol{v}}|^2}{\hat{T}} - \frac{\hat{\mathcal{E}}}{\hat{T}}\right), \tag{29}$$

where $\hat{\rho}$, $\hat{\boldsymbol{v}}$, and $\hat{T}$ are arbitrary functions of $\hat{t}$ and $\boldsymbol{x}$.

Conservation: For an arbitrary function $\hat{g}(\hat{t}, \boldsymbol{x}, \boldsymbol{\zeta}, \hat{\mathcal{E}})$, the relation

$$\iint_0^\infty \hat{\varphi}_r \hat{Q}(\hat{g}) d\hat{\mathcal{E}} d\boldsymbol{\zeta} = 0, \tag{30}$$

holds, where $\hat{\varphi}_r$ ($r = 0, ..., 4$) are the dimensionless collision invariants, i.e.,

$$\hat{\varphi}_0 = 1, \qquad \hat{\varphi}_i = \zeta_i \quad (i = 1, 2, 3), \qquad \hat{\varphi}_4 = |\boldsymbol{\zeta}|^2 + \hat{\mathcal{E}}. \tag{31}$$

Entropy inequality: For an arbitrary function $\hat{g}(\hat{t}, \boldsymbol{x}, \boldsymbol{\zeta}, \hat{\mathcal{E}})$, the following inequality holds:

$$\iint_0^\infty \left(\ln \frac{\hat{g}}{\hat{\mathcal{E}}^{\delta/2-1}}\right) \hat{Q}(\hat{g}) d\hat{\mathcal{E}} d\boldsymbol{\zeta} \le 0, \tag{32}$$

and the equality sign holds if and only if $\hat{g} = \hat{f}_{\rm eq}$ in (29).

B. Chapman–Enskog expansion and two-temperature Navier–Stokes equations

As mentioned in Sec. II E, we try to derive fluid-dynamic equations when not only the Knudsen number but also the parameter θ contained in the ES model is small. Therefore, we assume that θ is of the same order of magnitude as ϵ and let

$$\theta = \alpha\epsilon \ll 1, \tag{33}$$

where α is a positive constant (parameter) of the order of unity.

1. Preliminaries

If we formally let $\epsilon \to 0$, we have, from Eq. (24),

$$\hat{Q}(\hat{f})|_{\theta=0} = \hat{A}_c(\hat{T})\hat{\rho}\left(\hat{\mathcal{G}}|_{\theta=0} - \hat{f}\right) = 0, \tag{34}$$

because of Eq. (33). This equation essentially determines the form of the leading-order term of the Chapman–Enskog expansion [28] and the strategy of the expansion. Here, it is noted that the properties of the collision operator $\hat{Q}(\hat{f})|_{\theta=0}$ have been studied in Appendix A3 in [31]. The dimensionless versions of the equilibrium and the conservation laws are as follows:

Equilibrium: $\hat{Q}(\hat{f})|_{\theta=0} = 0$ is equivalent to the fact that $\hat{f}$ is the (dimensionless) local equilibrium of the form

$$\hat{f}_{\rm eq} = \frac{\bar{\rho}\,\hat{\mathcal{E}}^{\delta/2-1}}{(\pi\bar{T}_{\rm tr})^{3/2}\bar{T}_{\rm int}^{\delta/2}\Gamma(\delta/2)} \exp\left(-\frac{|\boldsymbol{\zeta}-\bar{\boldsymbol{v}}|^2}{\bar{T}_{\rm tr}} - \frac{\hat{\mathcal{E}}}{\bar{T}_{\rm int}}\right), \tag{35}$$

where $\bar{\rho}$, $\bar{\boldsymbol{v}}$, $\bar{T}_{\rm tr}$, and $\bar{T}_{\rm int}$ are arbitrary dimensionless functions of $\hat{t}$ and $\boldsymbol{x}$.

Conservation: For an arbitrary function $\hat{g}(\hat{t}, \boldsymbol{x}, \boldsymbol{\zeta}, \hat{\mathcal{E}})$, the relation

$$\iint_0^\infty \hat{\phi}_r \hat{Q}(\hat{g}) d\hat{\mathcal{E}} d\boldsymbol{\zeta} = 0, \tag{36}$$

holds, where $\hat{\phi}_r$ ($r = 0, ..., 5$) are the (dimensionless) collision invariants, i.e.,

$$\hat{\phi}_0 = 1, \qquad \hat{\phi}_i = \zeta_i \quad (i = 1, 2, 3), \qquad \hat{\phi}_4 = |\boldsymbol{\zeta}|^2, \qquad \hat{\phi}_5 = \hat{\mathcal{E}}. \tag{37}$$

Equation (35) shows that the local equilibrium $\hat{f}_{\rm eq}$ contains the six macroscopic quantities corresponding to collision invariants (37), i.e., the density $\hat{\rho}$, the flow velocity $\hat{\boldsymbol{v}}$, the temperature associated with the translational motion $\hat{T}_{\rm tr}$, and that associated with the internal modes $\hat{T}_{\rm int}$. This suggests that these are the basic quantities not to be expanded in ϵ in the Chapman–Enskog expansion and that the resulting fluid-dynamic equations corresponding to the Navier–Stokes equations are for these quantities.

Since $\hat{\rho}$, $\hat{\boldsymbol{v}}$, $\hat{T}_{\rm tr}$, and $\hat{T}_{\rm int}$ are directly related to the moments of $\hat{f}$ with $\hat{\phi}_r$ of Eq. (37), the fluid-dynamic equations should be obtained on the basis of the moment equations (or the weak form) of the ES model, Eq. (24) with Eq. (33), generated with these $\hat{\phi}_r$. To be more specific, multiplying Eq. (24) by $\hat{\phi}_r$ and integrating over the whole ranges of $\boldsymbol{\zeta}$ and $\hat{\mathcal{E}}$, we obtain the following moment equations.

$$\frac{\partial\hat{\rho}}{\partial\hat{t}} + \frac{\partial(\hat{\rho}\hat{v}_j)}{\partial x_j} = 0, \tag{38a}$$

$$\frac{\partial(\hat{\rho}\hat{v}_i)}{\partial\hat{t}} + \frac{\partial}{\partial x_j}\left(\hat{\rho}\hat{v}_i\hat{v}_j + \frac{1}{2}\hat{p}_{ij}\right) = 0, \tag{38b}$$

$$\frac{\partial}{\partial\hat{t}}\left[\hat{\rho}\left(\frac{3}{2}\hat{T}_{\rm tr} + \hat{v}_i^2\right)\right] + \frac{\partial}{\partial x_j}\left[\hat{\rho}\hat{v}_j\left(\frac{3}{2}\hat{T}_{\rm tr} + \hat{v}_i^2\right) + \hat{v}_i\hat{p}_{ij} + \hat{q}_{({\rm tr})j}\right] = \frac{3}{2}\alpha\hat{A}_c(\hat{T})\hat{\rho}^2(\hat{T} - \hat{T}_{\rm tr}), \tag{38c}$$

$$\frac{\partial}{\partial\hat{t}}\left(\frac{\delta}{2}\hat{\rho}\hat{T}_{\rm int}\right) + \frac{\partial}{\partial x_j}\left(\frac{\delta}{2}\hat{\rho}\hat{v}_j\hat{T}_{\rm int} + \hat{q}_{({\rm int})j}\right) = \frac{\alpha\delta}{2}\hat{A}_c(\hat{T})\hat{\rho}^2(\hat{T} - \hat{T}_{\rm int}). \tag{38d}$$

The right-hand sides of Eqs. (38c) and (38d) can be obtained readily from the moments of $\hat{f}$ and $\hat{\mathcal{G}}$ summarized in Appendix A in [31]. Equations (38a) and (38b) express the conservation of mass and momentum. If we add Eqs. (38c) and (38d) and take account of Eq. (25i), we recover the conservation of total energy, i.e.,

$$\frac{\partial}{\partial\hat{t}}\left[\hat{\rho}\left(\frac{3+\delta}{2}\hat{T} + \hat{v}_i^2\right)\right] + \frac{\partial}{\partial x_j}\left[\hat{\rho}\hat{v}_j\left(\frac{3+\delta}{2}\hat{T} + \hat{v}_i^2\right) + \hat{v}_i\hat{p}_{ij} + \hat{q}_j\right] = 0. \tag{39}$$

Therefore, only two equations are independent among Eqs. (38c), (38d), and (39).

The Chapman–Enskog expansion is a formal expansion of $\hat{f}$ in ϵ, i.e.,

$$\hat{f} = \hat{f}^{(0)} + \hat{f}^{(1)}\epsilon + \hat{f}^{(2)}\epsilon^2 + \cdots . \tag{40}$$

In the present problem, we impose the condition

$$\iint_0^\infty \hat{\phi}_r \hat{f}^{(m)} d\boldsymbol{\zeta} d\hat{\mathcal{E}} = 0, \qquad (r = 0, \dots, 5;\ m = 1, 2, \dots), \tag{41}$$

so that it follows from Eqs. (25d), (25e), (25g), and (25h) that

$$\hat{\rho} = \iint_0^\infty \hat{f}^{(0)} d\hat{\mathcal{E}} d\boldsymbol{\zeta}, \tag{42a}$$

$$\hat{v}_i = \frac{1}{\hat{\rho}} \iint_0^\infty \zeta_i \hat{f}^{(0)} d\hat{\mathcal{E}} d\boldsymbol{\zeta}, \tag{42b}$$

$$\hat{T}_{\rm tr} = \frac{2}{3\hat{\rho}} \iint_0^\infty (\zeta_k - \hat{v}_k)^2 \hat{f}^{(0)} d\hat{\mathcal{E}} d\boldsymbol{\zeta}, \tag{42c}$$

$$\hat{T}_{\rm int} = \frac{2}{\delta\hat{\rho}} \iint_0^\infty \hat{\mathcal{E}} \hat{f}^{(0)} d\hat{\mathcal{E}} d\boldsymbol{\zeta}. \tag{42d}$$

That is, $\hat{\rho}$, $\hat{v}_i$, $\hat{T}_{\rm tr}$, and $\hat{T}_{\rm int}$ are not expanded and are determined only by $\hat{f}^{(0)}$.

In accordance with Eq. (40), other macroscopic quantities $\hat{p}_{ij}$, $\hat{q}_i$, $\hat{q}_{({\rm tr})i}$, $\hat{q}_{({\rm int})i}$, and $\hat{T}_{\rm rel}$ are expanded as

$$h = h^{(0)} + h^{(1)}\epsilon + \cdots , \qquad (h = \hat{p}_{ij},\ \hat{q}_i,\ \hat{q}_{({\rm tr})i},\ \hat{q}_{({\rm int})i}, \text{ and } \hat{T}_{\rm rel}). \tag{43}$$

Here, the coefficients for $\hat{p}_{ij}$, $\hat{q}_i$, $\hat{q}_{({\rm tr})i}$, and $\hat{q}_{({\rm int})i}$ are obtained by substituting Eqs. (40) and (43) into Eqs. (25f) and (28), i.e.,

$$\hat{p}_{ij}^{(m)} = 2 \iint_0^\infty (\zeta_i - \hat{v}_i)(\zeta_j - \hat{v}_j) \hat{f}^{(m)} d\hat{\mathcal{E}} d\boldsymbol{\zeta}, \qquad (m = 0, 1, \dots), \tag{44}$$

and

$$\hat{q}_i^{(m)} = \hat{q}_{({\rm tr})i}^{(m)} + \hat{q}_{({\rm int})i}^{(m)}, \qquad (m = 0, 1, \dots), \tag{45a}$$

$$\hat{q}_{({\rm tr})i}^{(m)} = \iint_0^\infty (\zeta_i - \hat{v}_i) |\boldsymbol{\zeta} - \hat{\boldsymbol{v}}|^2 \hat{f}^{(m)} d\hat{\mathcal{E}} d\boldsymbol{\zeta}, \tag{45b}$$

$$\hat{q}_{({\rm int})i}^{(m)} = \iint_0^\infty (\zeta_i - \hat{v}_i) \hat{\mathcal{E}} \hat{f}^{(m)} d\hat{\mathcal{E}} d\boldsymbol{\zeta}, \tag{45c}$$

and those for $\hat{T}_{\rm rel}$ are obtained from Eqs. (25j) and (33), i.e.,

$$\hat{T}_{\rm rel}^{(0)} = \hat{T}_{\rm int}, \qquad \hat{T}_{\rm rel}^{(1)} = \alpha(\hat{T} - \hat{T}_{\rm int}), \qquad \hat{T}_{\rm rel}^{(m+2)} = 0, \qquad (m = 0, 1, \dots), \tag{46}$$

where $\hat{T}$ is determined by Eq. (25i) and thus is not expanded in ϵ.

If we substitute the expansion (40) into Eq. (24) with the setting Eq. (33), we obtain

$$[\hat{Q}(\hat{f})]^{(0)} = 0, \tag{47a}$$

$$[\hat{Q}(\hat{f})]^{(1)} = \frac{\partial \hat{f}^{(0)}}{\partial \hat{t}} + \zeta_j \frac{\partial \hat{f}^{(0)}}{\partial x_j} + O(\epsilon), \tag{47b}$$

where $[\hat{Q}(\hat{f})]^{(0)}$ and $[\hat{Q}(\hat{f})]^{(1)}$ are the coefficients of the expansion of the collision term $\hat{Q}(\hat{f})$ in ϵ:

$$\hat{Q}(\hat{f}) = [\hat{Q}(\hat{f})]^{(0)} + [\hat{Q}(\hat{f})]^{(1)}\epsilon + \cdots , \tag{48}$$

and are specified below. Since we consider only up to the first order solution $\hat{f} = \hat{f}^{(0)} + \hat{f}^{(1)}\epsilon$ in the following, the irrelevant higher-order terms are all put in the $O(\epsilon)$-term in Eq. (47b).

2. Zeroth-order solution

Because $[\hat{Q}(\hat{f})]^{(0)} = \hat{Q}(\hat{f})|_{\epsilon=0} = \hat{Q}(\hat{f})|_{\theta=0}$, the solution of the leading-order equation (47a) is given by Eq. (35), that is,

$$\hat{f}^{(0)} = \frac{\hat{\rho}\,\hat{\mathcal{E}}^{\delta/2-1}}{(\pi\hat{T}_{\rm tr})^{3/2}\hat{T}_{\rm int}^{\delta/2}\Gamma(\delta/2)} \exp\left(-\frac{|\boldsymbol{\zeta}-\hat{\boldsymbol{v}}|^2}{\hat{T}_{\rm tr}} - \frac{\hat{\mathcal{E}}}{\hat{T}_{\rm int}}\right), \tag{49}$$

where the arbitrary functions in Eq. (35) are determined in such a way that Eq. (42) holds. Using Eq. (49) in Eqs. (44) and (45), we have

$$\hat{p}_{ij}^{(0)} = \hat{\rho}\hat{T}_{\rm tr}\delta_{ij}, \qquad \hat{q}_{({\rm tr})i}^{(0)} = \hat{q}_{({\rm int})i}^{(0)} = \hat{q}_i^{(0)} = 0. \tag{50}$$

Therefore, we can write

$$\hat{p}_{ij} = \hat{\rho}\hat{T}_{\rm tr}\delta_{ij} + O(\epsilon), \qquad \hat{q}_{({\rm tr})i} = \hat{q}_{({\rm int})i} = \hat{q}_i = 0 + O(\epsilon). \tag{51}$$

The substitution of Eq. (51) into Eq. (38) leads to the following equations:

$$\frac{\partial\hat{\rho}}{\partial\hat{t}} + \frac{\partial(\hat{\rho}\hat{v}_j)}{\partial x_j} = 0, \tag{52a}$$

$$\frac{\partial(\hat{\rho}\hat{v}_i)}{\partial\hat{t}} + \frac{\partial(\hat{\rho}\hat{v}_i\hat{v}_j)}{\partial x_j} + \frac{1}{2}\frac{\partial(\hat{\rho}\hat{T}_{\rm tr})}{\partial x_i} = O(\epsilon), \tag{52b}$$

$$\frac{\partial}{\partial\hat{t}}\left[\hat{\rho}\left(\frac{3}{2}\hat{T}_{\rm tr} + \hat{v}_i^2\right)\right] + \frac{\partial}{\partial x_j}\left[\hat{\rho}\hat{v}_j\left(\frac{5}{2}\hat{T}_{\rm tr} + \hat{v}_i^2\right)\right] - \frac{3}{2}\alpha\hat{A}_c(\hat{T})\hat{\rho}^2(\hat{T}-\hat{T}_{\rm tr}) = O(\epsilon), \tag{52c}$$

$$\frac{\partial}{\partial\hat{t}}\left(\hat{\rho}\hat{T}_{\rm int}\right) + \frac{\partial}{\partial x_j}\left(\hat{\rho}\hat{v}_j\hat{T}_{\rm int}\right) - \alpha\hat{A}_c(\hat{T})\hat{\rho}^2(\hat{T}-\hat{T}_{\rm int}) = O(\epsilon), \tag{52d}$$

and the same substitution transforms Eq. (39) into

$$\frac{\partial}{\partial\hat{t}}\left[\hat{\rho}\left(\frac{3+\delta}{2}\hat{T} + \hat{v}_i^2\right)\right] + \frac{\partial}{\partial x_j}\left[\hat{\rho}\hat{v}_j\left(\frac{3+\delta}{2}\hat{T} + \hat{T}_{\rm tr} + \hat{v}_i^2\right)\right] = O(\epsilon). \tag{53}$$

Neglecting the terms of $O(\epsilon)$ in Eq. (52) and noting Eq. (25i), one obtains the system of partial differential equations for $\hat{\rho}$, $\hat{v}_i$, $\hat{T}_{\rm tr}$, and $\hat{T}_{\rm int}$ at the zeroth-order in ϵ. One of Eqs. (52c) and (52d) [without the $O(\epsilon)$-terms] can be replaced with Eq. (53) [without the $O(\epsilon)$-term]. These equations, whose steady version was derived in [31], correspond to the Euler system in the form of conservation laws with relaxation and are essentially the same as the macroscopic system for six macroscopic variables based on the extended thermodynamics derived in [21, 24] (ET6 system in the terminology in [21, 24]).

3. First-order solution

Next, we consider Eq. (47b) and calculate the terms on the right-hand side following the standard Chapman–Enskog procedure. The terms $\partial\hat{f}^{(0)}/\partial\hat{t}$ and $\partial\hat{f}^{(0)}/\partial x_j$ can be calculated explicitly by the use of Eq. (49), and the former is expressed in terms of the time derivatives $\partial\hat{\rho}/\partial\hat{t}$, $\partial\hat{v}_i/\partial\hat{t}$, $\partial\hat{T}_{\rm tr}/\partial\hat{t}$, and $\partial\hat{T}_{\rm int}/\partial\hat{t}$, whereas the latter in terms of the space derivatives $\partial\hat{\rho}/\partial x_j$, $\partial\hat{v}_i/\partial x_j$, $\partial\hat{T}_{\rm tr}/\partial x_j$, and $\partial\hat{T}_{\rm int}/\partial x_j$. It is reasonable to assume that Eq. (52) is still valid even if we proceed to the first order because we just make the $O(\epsilon)$-terms explicit with the first-order solution. From Eq. (52), we obtain the expression of the time derivative terms $\partial\hat{\rho}/\partial\hat{t}$, $\partial\hat{v}_i/\partial\hat{t}$, $\partial\hat{T}_{\rm tr}/\partial\hat{t}$, and $\partial\hat{T}_{\rm int}/\partial\hat{t}$ in terms of the space-derivative terms with the error of

$O(\epsilon)$. Using these expressions, we can eliminate the time-derivative terms arising from $\partial\hat{f}^{(0)}/\partial\hat{t}$ on the right-hand side of Eq. (47b). As the result, we have

$$\begin{aligned}
&\frac{1}{\hat{f}^{(0)}}\left(\frac{\partial\hat{f}^{(0)}}{\partial\hat{t}}+\zeta_j\frac{\partial\hat{f}^{(0)}}{\partial x_j}\right)\\
&\quad=\left[\frac{(\zeta_i-\hat{v}_i)(\zeta_j-\hat{v}_j)}{\hat{T}_{\rm tr}}-\frac{1}{3}\frac{(\zeta_k-\hat{v}_k)^2}{\hat{T}_{\rm tr}}\delta_{ij}\right]\left(\frac{\partial\hat{v}_i}{\partial x_j}+\frac{\partial\hat{v}_j}{\partial x_i}\right)\\
&\qquad+\frac{(\zeta_j-\hat{v}_j)}{\hat{T}_{\rm tr}}\left[\frac{(\zeta_k-\hat{v}_k)^2}{\hat{T}_{\rm tr}}-\frac{5}{2}\right]\frac{\partial\hat{T}_{\rm tr}}{\partial x_j}+\frac{(\zeta_j-\hat{v}_j)}{\hat{T}_{\rm int}}\left(\frac{\hat{\mathcal{E}}}{\hat{T}_{\rm int}}-\frac{\delta}{2}\right)\frac{\partial\hat{T}_{\rm int}}{\partial x_j}\\
&\qquad+\alpha\hat{A}_c(\hat{T})\hat{\rho}\left\{\left[\frac{(\zeta_k-\hat{v}_k)^2}{\hat{T}_{\rm tr}}-\frac{3}{2}\right]\left(\frac{\hat{T}}{\hat{T}_{\rm tr}}-1\right)+\left(\frac{\hat{\mathcal{E}}}{\hat{T}_{\rm int}}-\frac{\delta}{2}\right)\left(\frac{\hat{T}}{\hat{T}_{\rm int}}-1\right)\right\}\\
&\qquad+O(\epsilon).
\end{aligned}\tag{54}$$

The left-hand side of Eq. (47b) is

$$[\hat{Q}(\hat{f})]^{(1)}=\hat{A}_c(\hat{T})\hat{\rho}\left(\hat{\mathcal{G}}^{(1)}-\hat{f}^{(1)}\right),\tag{55}$$

where $\hat{\mathcal{G}}^{(1)}$ is the first-order term of the expansion of $\hat{\mathcal{G}}$ in ϵ, i.e.,

$$\hat{\mathcal{G}}=\hat{\mathcal{G}}^{(0)}+\hat{\mathcal{G}}^{(1)}\epsilon+\cdots.\tag{56}$$

Here, $\hat{\mathcal{G}}^{(0)}$ and $\hat{\mathcal{G}}^{(1)}$ are, respectively, expressed as

$$\hat{\mathcal{G}}^{(0)}=\hat{\mathcal{G}}|_{\epsilon=0},\qquad \hat{\mathcal{G}}^{(1)}=(d\hat{\mathcal{G}}/d\epsilon)|_{\epsilon=0},\tag{57}$$

and are calculated in Appendix A, according to which $\hat{\mathcal{G}}^{(1)}$ is obtained in the following form:

$$\begin{aligned}
\frac{1}{\hat{f}^{(0)}}\hat{\mathcal{G}}^{(1)}=&\nu\left[\frac{(\zeta_i-\hat{v}_i)(\zeta_j-\hat{v}_j)}{\hat{T}_{\rm tr}}-\frac{\delta_{ij}}{2}\right]\frac{\hat{p}_{ij}^{(1)}}{\hat{\rho}\hat{T}_{\rm tr}}\\
&+\alpha\left[\frac{(\zeta_k-\hat{v}_k)^2}{\hat{T}_{\rm tr}}-\frac{3}{2}\right]\left(\frac{\hat{T}}{\hat{T}_{\rm tr}}-1\right)+\alpha\left(\frac{\hat{\mathcal{E}}}{\hat{T}_{\rm int}}-\frac{\delta}{2}\right)\left(\frac{\hat{T}}{\hat{T}_{\rm int}}-1\right).
\end{aligned}\tag{58}$$

Using Eqs. (54), (55), and (58) in Eq. (47b) and neglecting the $O(\epsilon)$-terms, we obtain $\hat{f}^{(1)}$ in the following form:

$$\begin{aligned}
\hat{f}^{(1)}=&\nu\hat{f}^{(0)}\left[\frac{(\zeta_i-\hat{v}_i)(\zeta_j-\hat{v}_j)}{\hat{T}_{\rm tr}}-\frac{\delta_{ij}}{2}\right]\frac{\hat{p}_{ij}^{(1)}}{\hat{\rho}\hat{T}_{\rm tr}}\\
&-\frac{\hat{f}^{(0)}}{\hat{A}_c(\hat{T})\hat{\rho}}\left\{\left[\frac{(\zeta_i-\hat{v}_i)(\zeta_j-\hat{v}_j)}{\hat{T}_{\rm tr}}-\frac{1}{3}\frac{(\zeta_k-\hat{v}_k)^2}{\hat{T}_{\rm tr}}\delta_{ij}\right]\left(\frac{\partial\hat{v}_i}{\partial x_j}+\frac{\partial\hat{v}_j}{\partial x_i}\right)\right.\\
&\left.+\frac{(\zeta_j-\hat{v}_j)}{\hat{T}_{\rm tr}}\left[\frac{(\zeta_k-\hat{v}_k)^2}{\hat{T}_{\rm tr}}-\frac{5}{2}\right]\frac{\partial\hat{T}_{\rm tr}}{\partial x_j}+\frac{(\zeta_j-\hat{v}_j)}{\hat{T}_{\rm int}}\left(\frac{\hat{\mathcal{E}}}{\hat{T}_{\rm int}}-\frac{\delta}{2}\right)\frac{\partial\hat{T}_{\rm int}}{\partial x_j}\right\}.
\end{aligned}\tag{59}$$

Precisely speaking, this is the linear integral equation for $\hat{f}^{(1)}$ because $\hat{p}_{ij}^{(1)}$ is given by Eq. (44) with $m=1$. However, it should be noted that in Eq. (59), the functional form of $\hat{f}^{(1)}$ in terms of ζ_i and $\hat{\mathcal{E}}$ has already been determined. If we substitute Eq. (59) into Eq. (44) with $m=1$, we obtain the algebraic equation for $\hat{p}_{ij}^{(1)}$, which gives the following $\hat{p}_{ij}^{(1)}$:

$$\hat{p}_{ij}^{(1)}=-\frac{\hat{T}_{\rm tr}}{(1-\nu)\hat{A}_c(\hat{T})}\left(\frac{\partial\hat{v}_i}{\partial x_j}+\frac{\partial\hat{v}_j}{\partial x_i}-\frac{2}{3}\frac{\partial\hat{v}_k}{\partial x_k}\delta_{ij}\right).\tag{60}$$

By the substitution of this $\hat{p}_{ij}^{(1)}$, Eq. (59) is transformed to

$$\hat{f}^{(1)} = -\frac{1}{\hat{A}_c(\hat{T})\hat{\rho}}\hat{f}^{(0)}\Bigg\{\frac{1}{1-\nu}\left[\frac{(\zeta_i-\hat{v}_i)(\zeta_j-\hat{v}_j)}{\hat{T}_{\rm tr}}-\frac{1}{3}\frac{(\zeta_k-\hat{v}_k)^2}{\hat{T}_{\rm tr}}\delta_{ij}\right]\left(\frac{\partial\hat{v}_i}{\partial x_j}+\frac{\partial\hat{v}_j}{\partial x_i}\right)$$
$$+\frac{(\zeta_j-\hat{v}_j)}{\hat{T}_{\rm tr}}\left[\frac{(\zeta_k-\hat{v}_k)^2}{\hat{T}_{\rm tr}}-\frac{5}{2}\right]\frac{\partial\hat{T}_{\rm tr}}{\partial x_j}+\frac{(\zeta_j-\hat{v}_j)}{\hat{T}_{\rm int}}\left(\frac{\hat{\mathcal{E}}}{\hat{T}_{\rm int}}-\frac{\delta}{2}\right)\frac{\partial\hat{T}_{\rm int}}{\partial x_j}\Bigg\}. \tag{61}$$

It can be confirmed by the direct calculation that this $\hat{f}^{(1)}$ satisfies the constraint (41) with $m=1$. Therefore, Eq. (61) is the final form of $\hat{f}^{(1)}$.

Making use of Eq. (61), we can obtain $\hat{q}_{({\rm tr})i}^{(1)}$ and $\hat{q}_{({\rm int})i}^{(1)}$ from Eqs. (45b) and (45c), respectively. The result is as follows:

$$\hat{q}_{({\rm tr})i}^{(1)} = -\frac{5}{4}\frac{\hat{T}_{\rm tr}}{\hat{A}_c(\hat{T})}\frac{\partial\hat{T}_{\rm tr}}{\partial x_i},\qquad \hat{q}_{({\rm int})i}^{(1)} = -\frac{\delta}{4}\frac{\hat{T}_{\rm tr}}{\hat{A}_c(\hat{T})}\frac{\partial\hat{T}_{\rm int}}{\partial x_i}. \tag{62}$$

Summarizing Eqs. (50), (60), and (62), we can write

$$\hat{p}_{ij} = \hat{\rho}\hat{T}_{\rm tr}\delta_{ij} - \Gamma_\mu(\hat{T},\,\hat{T}_{\rm tr})\left(\frac{\partial\hat{v}_i}{\partial x_j}+\frac{\partial\hat{v}_j}{\partial x_i}-\frac{2}{3}\frac{\partial\hat{v}_k}{\partial x_k}\delta_{ij}\right)\epsilon+O(\epsilon^2), \tag{63a}$$

$$\hat{q}_{({\rm tr})i} = -\frac{5}{4}\Gamma_\lambda(\hat{T},\,\hat{T}_{\rm tr})\frac{\partial\hat{T}_{\rm tr}}{\partial x_i}\epsilon+O(\epsilon^2), \tag{63b}$$

$$\hat{q}_{({\rm int})i} = -\frac{\delta}{4}\Gamma_\lambda(\hat{T},\,\hat{T}_{\rm tr})\frac{\partial\hat{T}_{\rm int}}{\partial x_i}\epsilon+O(\epsilon^2), \tag{63c}$$

$$\hat{q}_i = \hat{q}_{({\rm tr})i}+\hat{q}_{({\rm int})i}, \tag{63d}$$

where

$$\Gamma_\mu(\hat{T},\,\hat{T}_{\rm tr}) = \frac{\hat{T}_{\rm tr}}{(1-\nu)\hat{A}_c(\hat{T})},\qquad \Gamma_\lambda(\hat{T},\,\hat{T}_{\rm tr}) = \frac{\hat{T}_{\rm tr}}{\hat{A}_c(\hat{T})}. \tag{64}$$

If we use Eq. (63) in Eq. (38), we obtain Eq. (52) with the explicit expressions of $O(\epsilon)$ terms and with the error of $O(\epsilon^2)$. By neglecting the error terms of $O(\epsilon^2)$, the higher-order equations for $\hat{\rho}$, $\hat{v}_i$, $\hat{T}_{\rm tr}$, and $\hat{T}_{\rm int}$ are obtained, i.e.,

$$\frac{\partial\hat{\rho}}{\partial\hat{t}}+\frac{\partial(\hat{\rho}\hat{v}_j)}{\partial x_j}=0, \tag{65a}$$

$$\frac{\partial(\hat{\rho}\hat{v}_i)}{\partial\hat{t}}+\frac{\partial(\hat{\rho}\hat{v}_i\hat{v}_j)}{\partial x_j}+\frac{1}{2}\frac{\partial(\hat{\rho}\hat{T}_{\rm tr})}{\partial x_i}=\frac{1}{2}\,\epsilon\frac{\partial}{\partial x_j}\left[\Gamma_\mu(\hat{T},\,\hat{T}_{\rm tr})\left(\frac{\partial\hat{v}_i}{\partial x_j}+\frac{\partial\hat{v}_j}{\partial x_i}-\frac{2}{3}\frac{\partial\hat{v}_k}{\partial x_k}\delta_{ij}\right)\right], \tag{65b}$$

$$\frac{\partial}{\partial\hat{t}}\left[\hat{\rho}\left(\frac{3}{2}\hat{T}_{\rm tr}+\hat{v}_i^2\right)\right]+\frac{\partial}{\partial x_j}\left[\hat{\rho}\hat{v}_j\left(\frac{5}{2}\hat{T}_{\rm tr}+\hat{v}_i^2\right)\right]-\frac{3}{2}\alpha\hat{A}_c(\hat{T})\hat{\rho}^2(\hat{T}-\hat{T}_{\rm tr})$$
$$=\frac{5}{4}\,\epsilon\frac{\partial}{\partial x_j}\left[\Gamma_\lambda(\hat{T},\,\hat{T}_{\rm tr})\frac{\partial\hat{T}_{\rm tr}}{\partial x_j}\right]+\epsilon\frac{\partial}{\partial x_j}\left[\Gamma_\mu(\hat{T},\,\hat{T}_{\rm tr})\hat{v}_i\left(\frac{\partial\hat{v}_i}{\partial x_j}+\frac{\partial\hat{v}_j}{\partial x_i}-\frac{2}{3}\frac{\partial\hat{v}_k}{\partial x_k}\delta_{ij}\right)\right], \tag{65c}$$

$$\frac{\partial(\hat{\rho}\hat{T}_{\rm int})}{\partial\hat{t}}+\frac{\partial(\hat{\rho}\hat{v}_j\hat{T}_{\rm int})}{\partial x_j}-\alpha\hat{A}_c(\hat{T})\hat{\rho}^2(\hat{T}-\hat{T}_{\rm int})=\frac{1}{2}\,\epsilon\frac{\partial}{\partial x_j}\left[\Gamma_\lambda(\hat{T},\,\hat{T}_{\rm tr})\frac{\partial\hat{T}_{\rm int}}{\partial x_j}\right], \tag{65d}$$

where $\hat{T}=(3\hat{T}_{\rm tr}+\delta\hat{T}_{\rm int})/(3+\delta)$ [Eq. (25i)]. Equations (65a)–(65d) correspond to the (compressible) Navier–Stokes equations in the case of the standard Chapman–Enskog expansion. Equation (39) (the total energy conservation), with Eq. (63) and with $O(\epsilon^2)$ terms being ne-

glected, becomes

$$\frac{\partial}{\partial \hat{t}}\left[\hat{\rho}\left(\frac{3+\delta}{2}\hat{T}+\hat{v}_i^2\right)\right]+\frac{\partial}{\partial x_j}\left[\hat{\rho}\hat{v}_j\left(\frac{3+\delta}{2}\hat{T}+\hat{T}_{\rm tr}+\hat{v}_i^2\right)\right]$$
$$=\frac{1}{2}\,\epsilon\frac{\partial}{\partial x_j}\left[\Gamma_\lambda(\hat{T},\,\hat{T}_{\rm tr})\left(\frac{3+\delta}{2}\frac{\partial \hat{T}}{\partial x_j}+\frac{\partial \hat{T}_{\rm tr}}{\partial x_j}\right)\right]$$
$$+\,\epsilon\frac{\partial}{\partial x_j}\left[\Gamma_\mu(\hat{T},\,\hat{T}_{\rm tr})\hat{v}_i\left(\frac{\partial \hat{v}_i}{\partial x_j}+\frac{\partial \hat{v}_j}{\partial x_i}-\frac{2}{3}\frac{\partial \hat{v}_k}{\partial x_k}\delta_{ij}\right)\right]. \tag{66}$$

Equation (66) may be used in place of Eq. (65c) or (65d). Equation (65), together with Eq. (66), is what we have called the *two-temperature* Navier–Stokes equations.

It should be mentioned that equations similar to Eq. (65) have been derived in [20, 25] from the Boltzmann equation. In [20], under the assumption that the collision integral is split into the rapid collision term and slow collision term, a system of Navier–Stokes equations with two temperatures is derived by the Chapman–Enskog method. The aim of the study is to clarify the effect of bulk viscosity, so that the collision term is written in a rather abstract form in terms of the collision cross sections (or the transition probabilities), whose explicit forms are not given. Therefore, it is not straightforward to apply the system to practical problems. On the other hand, [25] is specialized for CO_2 gas, and the detailed structure of a CO_2 molecule is taken into account in the collision terms. A system of Navier–Stokes equations with two temperatures is then derived by the Chapman–Enskog expansion. The system, whose transport properties are related to various collision cross sections, does not contain any adjustable parameters. However, it requires some calculated, empirical, or approximate formulas for application to CO_2 gas flows. It should be mentioned that the references [20, 25] provide important contributions in the field. However, our system (65), which takes the advantage of the simplicity of the ES model compared with the Boltzmann equation, has a simpler and explicit structure, so that its applicability to practical flow problems is much wider. An example of its application will be given in Sec. IV.

C. Summary

In Sec. III B, we derived the two-temperature Navier–Stokes equations by the Chapman–Enskog expansion for the ES model under the parameter setting (33). In the following, we summarize the dimensional form of the derived equations.

We start with the stress tensor p_{ij} and heat-flow vector q_i. With the help of Eq. (23), we can transform Eq. (63), with $O(\epsilon^2)$ terms being neglected, to the following dimensional form:

$$p_{ij}=\rho R T_{\rm tr}\delta_{ij}-\mu_{\rm tr}(T,\,T_{\rm tr})\left(\frac{\partial v_i}{\partial X_j}+\frac{\partial v_j}{\partial X_i}-\frac{2}{3}\frac{\partial v_k}{\partial X_k}\delta_{ij}\right), \tag{67a}$$

$$q_{({\rm tr})i}=-\lambda_{\rm tr}(T,\,T_{\rm tr})\frac{\partial T_{\rm tr}}{\partial X_i},\qquad q_{({\rm int})i}=-\lambda_{\rm int}(T,\,T_{\rm tr})\frac{\partial T_{\rm int}}{\partial X_i}, \tag{67b}$$

$$q_i=q_{({\rm tr})i}+q_{({\rm int})i}, \tag{67c}$$

where

$$\mu_{\rm tr}(T,\,T_{\rm tr})=\frac{1}{1-\nu}\frac{RT_{\rm tr}}{A_c(T)},\quad \lambda_{\rm tr}(T,\,T_{\rm tr})=\frac{5}{2}R\frac{RT_{\rm tr}}{A_c(T)},\quad \lambda_{\rm int}(T,\,T_{\rm tr})=\frac{\delta}{2}R\frac{RT_{\rm tr}}{A_c(T)}, \tag{68}$$

and $T=(3T_{\rm tr}+\delta T_{\rm int})/(3+\delta)$ [Eq. (4i)]. In deriving Eq. (67), use has been made of Eqs. (12) and (26). The stress tensor p_{ij} contains the *pressure* $\rho R T_{\rm tr}$ based on the translational temperature, and $\mu_{\rm tr}$ plays the role of (shear) viscosity. The bulk viscosity does not appear in p_{ij}. The coefficient $\lambda_{\rm tr}$ and $\lambda_{\rm int}$ are, respectively, the thermal conductivity for the translational temperature and that for the internal temperature. Note that the Fourier law (13b) does not hold in this case.

Then, Eqs. (65) are transformed into the following dimensional two-temperature Navier–

Stokes equations:

$$\frac{\partial \rho}{\partial t} + \frac{\partial (\rho v_j)}{\partial X_j} = 0, \tag{69a}$$

$$\frac{\partial (\rho v_i)}{\partial t} + \frac{\partial (\rho v_i v_j)}{\partial X_j} + \frac{\partial (\rho R T_{\rm tr})}{\partial X_i} = \frac{\partial}{\partial X_j}\left[\mu(T,\, T_{\rm tr})\left(\frac{\partial v_i}{\partial X_j} + \frac{\partial v_j}{\partial X_i} - \frac{2}{3}\frac{\partial v_k}{\partial X_k}\delta_{ij}\right)\right], \tag{69b}$$

$$\begin{aligned}\frac{\partial}{\partial t}\left[\rho\left(\frac{3}{2}RT_{\rm tr} + \frac{1}{2}v_i^2\right)\right] + \frac{\partial}{\partial X_j}\left[\rho v_j\left(\frac{5}{2}RT_{\rm tr} + \frac{1}{2}v_i^2\right)\right] - \frac{3}{2}\theta A_c(T)\rho^2 R(T - T_{\rm tr}) \\ = \frac{\partial}{\partial X_j}\left[\lambda_{\rm tr}(T,\, T_{\rm tr})\frac{\partial T_{\rm tr}}{\partial X_j}\right] + \frac{\partial}{\partial X_j}\left[\mu_{\rm tr}(T,\, T_{\rm tr})v_i\left(\frac{\partial v_i}{\partial X_j} + \frac{\partial v_j}{\partial X_i} - \frac{2}{3}\frac{\partial v_k}{\partial X_k}\delta_{ij}\right)\right],\end{aligned} \tag{69c}$$

$$\frac{\partial (\rho T_{\rm int})}{\partial t} + \frac{\partial (\rho v_j T_{\rm int})}{\partial X_j} - \theta A_c(T)\rho^2(T - T_{\rm int}) = \frac{2}{\delta}\frac{1}{R}\frac{\partial}{\partial X_j}\left[\lambda_{\rm int}(T,\, T_{\rm int})\frac{\partial T_{\rm int}}{\partial X_j}\right]. \tag{69d}$$

These are the equations for ρ, v_i, $T_{\rm tr}$, and $T_{\rm int}$. If Eq. (69d) is multiplied by $(\delta/2)R$, the unit becomes consistent with Eq. (69c). It should be noted that the parameter θ ($\theta \ll 1$) contained in the ES model [cf. Eqs. (4c) and (4j)] appears in Eqs. (69c) and (69d). In addition, the equation for the total energy (66) is transformed to

$$\begin{aligned}&\frac{\partial}{\partial t}\left[\rho\left(\frac{3+\delta}{2}RT + \frac{1}{2}v_i^2\right)\right] + \frac{\partial}{\partial X_j}\left[\rho v_j\left(\frac{3+\delta}{2}RT + RT_{\rm tr} + \frac{1}{2}v_i^2\right)\right] \\ &\quad = \frac{2}{5}\frac{\partial}{\partial X_j}\left[\lambda_{\rm tr}(T,\, T_{\rm tr})\left(\frac{3+\delta}{2}\frac{\partial T}{\partial X_j} + \frac{\partial T_{\rm tr}}{\partial X_j}\right)\right] \\ &\qquad + \frac{\partial}{\partial X_j}\left[\mu_{\rm tr}(T,\, T_{\rm tr})v_i\left(\frac{\partial v_i}{\partial X_j} + \frac{\partial v_j}{\partial X_i} - \frac{2}{3}\frac{\partial v_k}{\partial X_k}\delta_{ij}\right)\right].\end{aligned} \tag{70}$$

This can also be derived directly by adding (69c) and (69d)$\times(\delta/2)R$. Therefore, Eq. (69c) or (69d) can be replaced by Eq. (70).

IV. APPLICATION TO SHOCK-WAVE STRUCTURE

In this section, we apply the two-temperature Navier–Stokes equations, Eq. (65), derived in Sec. III to the problem of shock-wave structure for CO_2 gas. A shock wave is a compression wave across which physical quantities undergo rapid changes over a distance of some tens of the mean free path. Therefore, the study of the structure inside the shock wave requires kinetic theory or, more specifically, the Boltzmann equation. In fact, the structure of a stationary plane shock wave is one of the most fundamental problems in kinetic theory and has been investigated by many authors. Since the survey of existing work is beyond the scope of the present paper, we just refer to some standard textbooks [1, 36, 47–50] containing this subject.

On the other hand, there have been several attempts to tackle this problem with macroscopic equations that are beyond the Navier–Stokes equations and are claimed to be valid for nonequilibrium flows (see [23, 51, 52] and the references therein) because the macroscopic equations are much more tractable than the original Boltzmann equation. In particular, when a polyatomic gas is considered, the approach using the Boltzmann equation is not practical because of insufficient information on the collision process of gas molecules. In this case, therefore, the approach using macroscopic equations, as well as that using model Boltzmann equations with simplified collision integrals, is more practical and powerful.

Let us restrict ourselves to the case of a polyatomic gas. Such an approach using macroscopic equations was considered in [23, 32–35, 53] rather recently, and some interesting results were reported. More specifically, the macroscopic equations based on the extended thermodynamics were used to investigate the shock-structure problem for CO_2 gas, which is known to have a large ratio of the bulk viscosity to the viscosity (cf. Sec. II E). It was shown numerically that the shock wave is very thick and there were three different types of profiles of the macroscopic quantities depending on the upstream Mach number. Subsequently, these results were confirmed by the numerical analysis based on kinetic theory using the ES model in [18, 30, 31]. It should also be mentioned that the problem has been tackled with various macroscopic equations of the Euler and Navier–Stokes types derived from the Boltzmann equation for CO_2 gas [25, 57, 58].

Now, let us recall that the two-temperature Navier–Stokes equations (65) [or Eq. (69)] have been derived from the ES model when the parameter θ is small. As discussed in Sec. II E, this corresponds to large values of the ratio of the bulk viscosity to the viscosity or to slow relaxation of the internal modes. Therefore, it is natural to expect that the two-temperature Navier–Stokes equations are able to describe the shock-wave structure for CO_2 gas. For this reason, we try to analyze the shock-structure problem for CO_2 gas numerically using Eq. (65). It should be noted that the present two-temperature Navier–Stokes equations have a different structure from the macroscopic equations used in [23, 32–35].

A. Problem

We consider a stationary plane shock wave in a flow of an ideal polyatomic gas with slow relaxation of the internal modes, perpendicular to the shock wave. The X_1 axis of the coordinate system is taken in the flow direction. The gas at upstream infinity ($X_1 \to -\infty$) is in an equilibrium state with density ρ_-, flow velocity $\boldsymbol{v}_- = (v_-, 0, 0)$, and temperature T_-, and that at downstream infinity ($X_1 \to +\infty$) is in another equilibrium state with density ρ_+, flow velocity $\boldsymbol{v}_+ = (v_+, 0, 0)$, and temperature T_+. These upstream and downstream parameters are related by the Rankine–Hugoniot relations. We investigate the steady behavior of the gas under the following assumptions:

(i) The behavior of the gas is described by the two-temperature Navier–Stokes equations derived in Sec. III B.

(ii) The problem is spatially one dimensional, so that the physical quantities are independent of X_2 and X_3.

Let M_- denote the Mach number of the flow at upstream infinity, i.e.,

$$M_- = \frac{v_-}{\sqrt{\gamma R T_-}}, \tag{71}$$

where $\gamma = c_p/c_v$ is the ratio of the specific heats already appeared in Sec. II A [cf. Eq. (1)]. Then, the Rankine–Hugoniot relations provide the following expressions of the downstream quantities ρ_+, v_+, and T_+ in terms of the upstream quantities ρ_-, v_-, and T_- and the upstream Mach number M_-:

$$\rho_+ = \frac{(\gamma+1)M_-^2}{(\gamma-1)M_-^2+2}\,\rho_-, \tag{72a}$$

$$v_+ = \frac{(\gamma-1)M_-^2+2}{(\gamma+1)M_-^2}\,v_-, \tag{72b}$$

$$T_+ = \frac{[2\gamma M_-^2-(\gamma-1)][(\gamma-1)M_-^2+2]}{(\gamma+1)^2 M_-^2}\,T_-. \tag{72c}$$

Incidentally, the Mach number of the flow at downstream infinity M_+, i.e., $M_+ = v_+/\sqrt{\gamma R T_+}$, is given as

$$M_+ = \left[\frac{(\gamma-1)M_-^2+2}{2\gamma M_-^2-(\gamma-1)}\right]^{1/2}. \tag{73}$$

B. Basic equations

We apply the two-temperature Navier–Stokes equations (65) to the present problem. In this connection, we should specify the appropriate reference quantities. In the following, we take ρ_0, T_0, and p_0 as

$$\rho_0 = \rho_-, \qquad T_0 = T_-, \qquad p_0 = p_- = R\rho_- T_-, \tag{74}$$

so that the reference mean free path l_0 becomes the following l_-, i.e.,

$$l_0 = l_- = \frac{2}{\sqrt{\pi}} \frac{(2RT_-)^{1/2}}{A_c(T_-)\rho_-}. \tag{75}$$

Since the problem is a steady and one-dimensional one with a unidirectional flow, we let $\partial/\partial\hat{t} = \partial/\partial x_2 = \partial/\partial x_3 = 0$ and $\hat{v}_2 = \hat{v}_3 = 0$.

In the present problem, the only characteristic length is the mean free path l_-, and there is no reference length L. Therefore, the small parameter $\epsilon = (\sqrt{\pi}/2)(l_-/L)$ does not make sense. However, by an appropriate scaling of the space coordinate, we can naturally eliminate the *fake* small parameter ϵ from Eqs. (65). Let us take an arbitrary number much larger than l_-, regard this number as L, and define ϵ by $\epsilon = (\sqrt{\pi}/2)(l_-/L)$. Then, we introduce a new space coordinate η in place of x_1 as

$$\eta = \frac{x_1}{\epsilon} = \frac{2}{\sqrt{\pi}} \frac{X_1}{l_-}. \tag{76}$$

This means that η is the X_1 coordinate normalized by the quantity of the order of the mean free path l_-. By changing the space coordinate from x_1 to η and using Eqs. (25i), (64), and (33), we can transform the time-independent and one-dimensional version of Eq. (65) to the following form:

$$\frac{d(\hat{\rho}\hat{v}_1)}{d\eta} = 0, \tag{77a}$$

$$\frac{d(\hat{\rho}\hat{v}_1^2)}{d\eta} = -\frac{1}{2}\frac{d(\hat{\rho}\hat{T}_{\rm tr})}{d\eta} + \frac{2}{3(1-\nu)}\frac{d}{d\eta}\left[\frac{\hat{T}_{\rm tr}}{\hat{A}_c(\hat{T})}\frac{d\hat{v}_1}{d\eta}\right], \tag{77b}$$

$$\begin{aligned}\frac{d}{d\eta}\left[\hat{\rho}\hat{v}_1\left(\frac{5}{2}\hat{T}_{\rm tr} + \hat{v}_1^2\right)\right] + \frac{3\delta}{2(3+\delta)}\theta\hat{A}_c(\hat{T})\hat{\rho}^2\left(\hat{T}_{\rm tr} - \hat{T}_{\rm int}\right) \\ = \frac{5}{4}\frac{d}{d\eta}\left[\frac{\hat{T}_{\rm tr}}{\hat{A}_c(\hat{T})}\frac{d\hat{T}_{\rm tr}}{d\eta}\right] + \frac{4}{3(1-\nu)}\frac{d}{d\eta}\left[\frac{\hat{T}_{\rm tr}}{\hat{A}_c(\hat{T})}\hat{v}_1\frac{d\hat{v}_1}{d\eta}\right],\end{aligned} \tag{77c}$$

$$\frac{d}{d\eta}\left(\hat{\rho}\hat{v}_1\hat{T}_{\rm int}\right) + \frac{3}{(3+\delta)}\theta\hat{A}_c(\hat{T})\hat{\rho}^2\left(\hat{T}_{\rm int} - \hat{T}_{\rm tr}\right) = \frac{1}{2}\frac{d}{d\eta}\left[\frac{\hat{T}_{\rm tr}}{\hat{A}_c(\hat{T})}\frac{d\hat{T}_{\rm int}}{d\eta}\right]. \tag{77d}$$

As we can see, the parameter ϵ does not occur in Eq. (77), and only the original small parameter θ appears in Eqs. (77c) and (77d).

Our problem is to solve Eq. (77) under the following boundary conditions:

$$(\hat{\rho}, \hat{v}_1, \hat{T}_{\rm tr}, \hat{T}_{\rm int}) \to (1, \hat{v}_-, 1, 1) \qquad \text{as} \quad \eta \to -\infty, \tag{78a}$$

$$\to (\hat{\rho}_+, \hat{v}_+, \hat{T}_+, \hat{T}_+) \qquad \text{as} \quad \eta \to \infty, \tag{78b}$$

where $\hat{\rho}_+ = \rho_+/\rho_-$, $\hat{v}_\pm = v_\pm/(2RT_-)^{1/2}$, and $\hat{T}_+ = T_+/T_-$. Since $\hat{v}_- = (\gamma/2)^{1/2}M_-$ [cf. Eq. (71)], the dimensionless downstream parameters $\hat{\rho}_+$, $\hat{v}_+$, and $\hat{T}_+$ are expressed in terms of M_- by the Rankine–Hugoniot relations (72).

C. Numerical method

In this section, we try to solve the boundary-value problem of the system of ordinary differential equations, Eqs. (77) and (78), numerically. For this purpose, we introduce the new (dimensionless) time variable $\bar{t}$, i.e.,

$$\bar{t} = \hat{t}/\epsilon, \tag{79}$$

add the corresponding time-derivative terms [cf. Eq. (65)], i.e.,

$$\frac{\partial\hat{\rho}}{\partial\bar{t}}, \qquad \frac{\partial(\hat{\rho}\hat{v}_1)}{\partial\bar{t}}, \qquad \frac{\partial}{\partial\bar{t}}\left[\hat{\rho}\left(\frac{3}{2}\hat{T}_{\rm tr} + \hat{v}_1^2\right)\right], \qquad \frac{\partial(\hat{\rho}\hat{T}_{\rm int})}{\partial\bar{t}}, \tag{80}$$

to the left-hand sides of Eqs. (77a)–(77d), respectively, and replace $d/d\eta$ with $\partial/\partial\eta$ in these equations. Then, we solve the resulting system, under an appropriate initial condition and the boundary condition (78), to pursue the time evolution of the solution and regard the long-time limit as the solution of Eqs. (77) and (78).

For simplicity, we change the notation as

$$(\bar{t},\, \hat{\rho},\, \hat{v}_1,\, \hat{T}_{\rm tr},\, \hat{T}_{\rm int},\, \hat{T},\, \hat{A}_c) \Rightarrow (t,\, \rho,\, v,\, T_{\rm tr},\, T_{\rm int},\, T,\, A_c), \tag{81}$$

only in this subsection. The quantities on the right-hand side of Eq. (81) should not be confused with the original dimensional quantities with the same symbols.

Our time-dependent equations can be written in the following form:

$$\frac{\partial U}{\partial t} + \frac{\partial F}{\partial \eta} = \frac{\partial G}{\partial \eta} + \theta H, \tag{82}$$

where

$$U = \begin{bmatrix} \rho \\ \rho v \\ \rho\left(\dfrac{3}{2}T_{\rm tr} + v^2\right) \\ \rho T_{\rm int} \end{bmatrix}, \quad F = \begin{bmatrix} \rho v \\ \rho v^2 + \dfrac{1}{2}\rho T_{\rm tr} \\ \rho v\left(\dfrac{5}{2}T_{\rm tr} + v^2\right) \\ \rho v T_{\rm int} \end{bmatrix}, \tag{83a}$$

$$G = \begin{bmatrix} 0 \\ \dfrac{2}{3(1-\nu)}\dfrac{T_{\rm tr}}{A_c(T)}\dfrac{\partial v}{\partial \eta} \\ \dfrac{5}{4}\dfrac{T_{\rm tr}}{A_c(T)}\dfrac{\partial T_{\rm tr}}{\partial \eta} + \dfrac{4}{3(1-\nu)}\dfrac{T_{\rm tr}}{A_c(T)}v\dfrac{\partial v}{\partial \eta} \\ \dfrac{1}{2}\dfrac{T_{\rm tr}}{A_c(T)}\dfrac{\partial T_{\rm int}}{\partial \eta} \end{bmatrix}, \quad H = \begin{bmatrix} 0 \\ 0 \\ \dfrac{3\delta}{2(3+\delta)}A_c(T)\rho^2(T_{\rm int} - T_{\rm tr}) \\ \dfrac{3}{3+\delta}A_c(T)\rho^2(T_{\rm tr} - T_{\rm int}) \end{bmatrix}, \tag{83b}$$

and $T = (3T_{\rm tr} + \delta T_{\rm int})/(3+\delta)$. We solve this system under the boundary conditions

$$(\rho,\, v,\, T_{\rm tr},\, T_{\rm int}) \to \begin{cases} (1,\, \hat{v}_-,\, 1,\, 1) & \text{as} \quad \eta \to -\infty, \\ (\hat{\rho}_+,\, \hat{v}_+,\, \hat{T}_+,\, \hat{T}_+) & \text{as} \quad \eta \to \infty, \end{cases} \tag{84}$$

and the following initial condition:

$$\begin{aligned} &\rho = 1 + \frac{\hat{\rho}_+ - 1}{2}\left[\tanh\bigl(a(\eta - b)\bigr) + 1\right], \qquad v = \hat{v}_-/\rho, \\ &T_{\rm tr} = T_{\rm int} = \left[1 + 2\hat{v}_-(\hat{v}_- - v)\right]/\rho, \end{aligned} \tag{85}$$

where a and b are the parameters that adjust the position and gradient of the initial wave front and are chosen appropriately depending on the computational conditions. The v and T ($= T_{\rm tr} = T_{\rm int}$) in Eq. (85) are determined using the first two lines of $\partial F/\partial\eta = 0$ [cf. Eq. (83a)].

We solve this problem by a finite-difference method with the MacCormack scheme [54, 55]. We restrict the domain to $-D_n \le \eta \le D_p$ and set the grid points η_i ($i = -N_n, -N_n + 1, \ldots, 0, \ldots, N_p - 1, N_p$) in such a way that $\eta_{-N_n} = -D_n$, $\eta_0 = 0$, and $\eta_{N_p} = D_p$. Let $\eta_{i-1/2}$ denote the middle point of the interval $[\eta_{i-1},\, \eta_i]$, i.e., $\eta_{i-1/2} = (\eta_{i-1} + \eta_i)/2$, $\Delta\eta_i$ the length of the grid interval $[\eta_{i-1},\, \eta_i]$, i.e., $\Delta\eta_i = \eta_i - \eta_{i-1}$, and t_n ($n = 0, 1, 2, \ldots$) the discrete time, i.e., $t_n = n\Delta t$ with Δt being the constant time step. In addition, we denote by h_i^n the value of the function $h(t, \eta)$ at $t = t_n$ and $\eta = \eta_i$, where h indicates ρ, v, $T_{\rm tr}$, etc. That is,

$$h_i^n = h(t_n,\, \eta_i), \qquad (h = \rho,\, v,\, T_{\rm tr},\, T_{\rm int},\, T,\, U,\, F,\, G, \text{ and } H), \tag{86}$$

with $i = -N_n, -N_n + 1, \ldots, 0, \ldots, N_p - 1, N_p$ and $n = 0, 1, 2, \ldots$.

We discretize Eq. (82) using the MacCormack scheme with a predictor-corrector step. That is, for $i = -N_n + 1, -N_n + 2, \dots, 0, \dots, N_p - 2, N_p - 1$,

$$U_i^* = \begin{cases} U_i^n - \dfrac{\Delta t}{\Delta\eta_i}\left(F_i^n - F_{i-1}^n\right), \quad (\text{for } U = \rho,\ i = N_p - 1), \\ U_i^n - \dfrac{\Delta t}{\Delta\eta_{i+1}}\left(F_{i+1}^n - F_i^n\right) + \dfrac{\Delta t}{\Delta\eta_{i+1/2}}\left(G_{i+1/2}^n - G_{i-1/2}^n\right) + \Delta t\ \theta H_i^n, \\ \qquad\qquad (\text{otherwise}), \end{cases} \tag{87a}$$

$$U_i^{n+1} = \frac{1}{2}\left[(U_i^n + U_i^*) - \frac{\Delta t}{\Delta\eta_i}\left(F_i^* - F_{i-1}^*\right) + \frac{\Delta t}{\Delta\eta_{i+1/2}}\left(G_{i+1/2}^* - G_{i-1/2}^*\right) + \Delta t\ \theta H_i^*\right], \tag{87b}$$

where F_i^*, G_i^*, and H_i^* are the values of F_i, G_i, and H_i based on the values of U_i^* (or the corresponding values of ρ_i^*, v_i^*, $T_{\mathrm{tr},i}^*$, $T_{\mathrm{int},i}^*$, and T_i^*), and

$$G_{i-1/2}^n = \begin{bmatrix} 0 \\ \dfrac{2}{3(1-\nu)}\dfrac{T_{\mathrm{tr},i-1/2}^n}{A_c(T_{i-1/2}^n)}\dfrac{v_i^n - v_{i-1}^n}{\Delta\eta_i} \\ \dfrac{5}{4}\dfrac{T_{\mathrm{tr},i-1/2}^n}{A_c(T_{i-1/2}^n)}\dfrac{T_{\mathrm{tr},i}^n - T_{\mathrm{tr},i-1}^n}{\Delta\eta_i} + \dfrac{4}{3(1-\nu)}\dfrac{T_{\mathrm{tr},i-1/2}^n}{A_c(T_{i-1/2}^n)}v_{i-1/2}^n\dfrac{v_i^n - v_{i-1}^n}{\Delta\eta_i} \\ \dfrac{1}{2}\dfrac{T_{\mathrm{tr},i-1/2}^n}{A_c(T_{i-1/2}^n)}\dfrac{T_{\mathrm{int},i}^n - T_{\mathrm{int},i-1}^n}{\Delta\eta_i} \end{bmatrix}. \tag{88}$$

As we see below, U_i^* is the predicted values, and U_i^{n+1} is the corrected values at time t_{n+1}.

Corresponding to the initial condition (85) and the condition at infinity (84), we set, for any i,

$$\begin{aligned} &\rho_i^0 = 1 + \frac{\hat\rho_+ - 1}{2}\left[\tanh\big(a(\eta_i - b)\big) + 1\right], \qquad v_i^0 = \hat v_-/\rho_i^0, \\ &T_{\mathrm{tr},i}^0 = T_{\mathrm{int},i}^0 = \left[1 + 2\hat v_-(\hat v_- - v_i^0)\right]/\rho_i^0, \end{aligned} \tag{89}$$

and, for any n,

$$\rho_{-N_n}^n = 1, \qquad v_{-N_n}^n = \hat v_-, \qquad T_{\mathrm{tr},-N_n}^n = T_{\mathrm{int},-N_n}^n = T_{-N_n}^n = 1, \tag{90a}$$

$$\rho_{N_p}^n = \hat\rho_+, \qquad v_{N_p}^n = \hat v_+, \qquad T_{\mathrm{tr},N_p}^n = T_{\mathrm{int},N_p}^n = T_{N_p}^n = \hat T_+. \tag{90b}$$

Suppose that the values of h_i^n at time t_n is known, where $h = \rho$, v, T_{tr}, T_{int}, and T, and $i = -N_n, -N_n + 1, \dots, N_p - 1, N_p$. Then, the values h_i^{n+1} at time t_{n+1} are obtained by the following procedure:

(i) We obtain the values $v_{i-1/2}^n, T_{\mathrm{tr},i-1/2}^n, T_{i-1/2}^n$ $(i = -N_n+1, -N_n+2, \dots, N_p)$ at the middle points $\eta_{i-1/2}$ by the linear interpolation.

(ii) We obtain U_i^n, F_i^n, and H_i^n $(i = -N_n, -N_n + 1, \dots, N_p)$ from Eq. (83) and $G_{i-1/2}^n$ $(i = -N_n + 1, -N_n + 2, \dots, N_p)$ from Eq. (88).

(iii) We obtain U_i^* $(i = -N_n + 1, -N_n + 2, \dots, N_p - 1)$ from Eq. (87a).

(iv) We obtain h_i^* $(i = -N_n + 1, -N_n + 2, \dots, N_p - 1)$ from the first equation of Eq. (83a). Here, we assume that $h_{-N_n}^* = h_{-N_n}^n$ and $h_{N_p}^* = h_{N_p}^n$.

(v) Similarly to the processes (i) and (ii), we obtain F_i^*, H_i^* $(i = -N_n, -N_n+1, \dots, N_p)$ and $G_{i-1/2}^*$ $(i = -N_n + 1, -N_n + 2, \dots, N_p)$.

(vi) We obtain U_i^{n+1} $(i = -N_n + 1, -N_n + 2, \dots, N_p - 1)$ from Eq. (87b) and h_i^{n+1} $(i = -N_n + 1, -N_n + 2, \dots, N_p - 1)$ from the first equation of Eq. (83a).

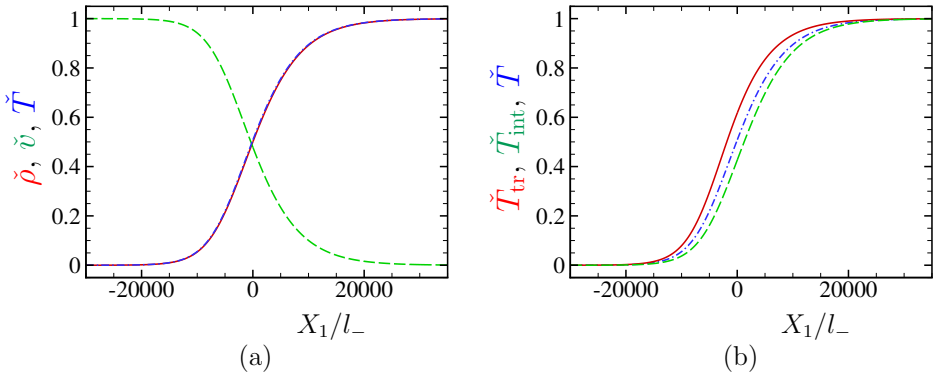

FIG. 1: Profiles of $\check{\rho}$, $\check{v}$, $\check{T}$, $\check{T}_{\rm tr}$, and $\check{T}_{\rm int}$ at $M_- = 1.05$ for $\mu_b/\mu = 1000$. In (a), the red solid line indicates $\check{\rho}$, the green dashed line $\check{v}$, and the blue dot-dashed line $\check{T}$, and in (b), the red solid line indicates $\check{T}_{\rm tr}$, the green dashed line $\check{T}_{\rm int}$, and the blue dot-dashed line $\check{T}$.

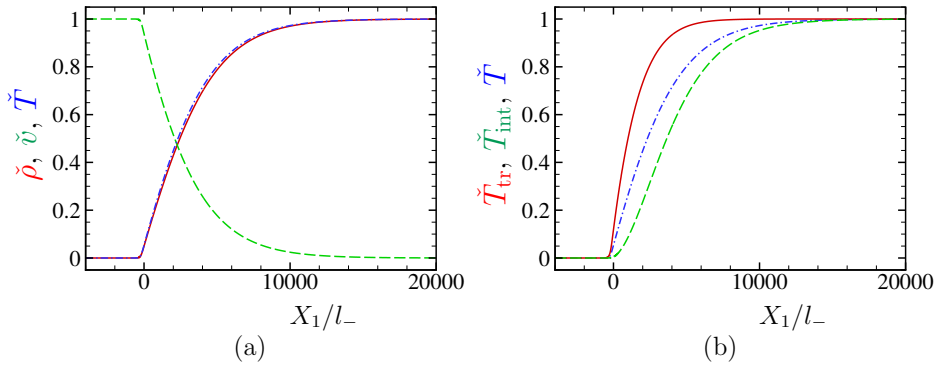

FIG. 2: Profiles of $\check{\rho}$, $\check{v}$, $\check{T}$, $\check{T}_{\rm tr}$, and $\check{T}_{\rm int}$ at $M_- = 1.138$ for $\mu_b/\mu = 1000$. See the caption of Fig. 1.

Starting from $n = 0$, we repeat the processes (i)–(vi) until the solution can be regarded as the steady solution. In this way, we obtain the solution of Eqs. (77) and (78).

We should note that the scheme for ρ_i^* at $i = N_p - 1$ [the first line of Eq. (87a)] uses a backward finite difference for the η-derivative in contrast to the other cases [the second line of Eq. (87a)] where a forward difference is used. This is because the constraint $\rho_{N_p}^n = \hat{\rho}_+$ is not compatible with the hyperbolic equation, the first row of (82), with positive v. If a forward difference for the η-derivative is used in the first line of Eq. (87a), the constraint $\rho_{N_p}^n = \hat{\rho}_+$ causes an oscillation, which propagates upstream. This inconvenience can be avoided by the scheme (87a) with the backward finite difference.

We can, in principle, solve the steady system, Eqs. (77) and (78), directly to obtain the steady shock profile by using Runge–Kutta method. However, perhaps because of the weak stability of the downstream equilibrium state, this approach turned out to be quite difficult. The same is true for the ordinary Navier–Stokes equations (with one temperature) [56]. Therefore, we adopted the time-dependent approach.

D. Numerical result

In this section, we show some results for CO_2 gas obtained using the two-temperature Navier–Stokes equations. In order to compare the results with those based on the kinetic ES model obtained in [31], we use the same parameter setting as in [31]. To be more specific, we let $\delta = 4$ ($\gamma = 9/7$), Pr $= 0.761$, and $A_c(T) =$ const [i.e., $\hat{A}_c(\hat{T}) = 1$]. As mentioned in Sec. II E, the ratio μ_b/μ of the bulk viscosity μ_b to the viscosity μ is as large as 1000 for CO_2 gas [42]. In [31], however, an artificial CO_2 gas, called *pseudo*-CO_2 gas, with variable ratio μ_b/μ was considered for the purpose of studying the behavior of the shock profiles when μ_b/μ becomes large. In

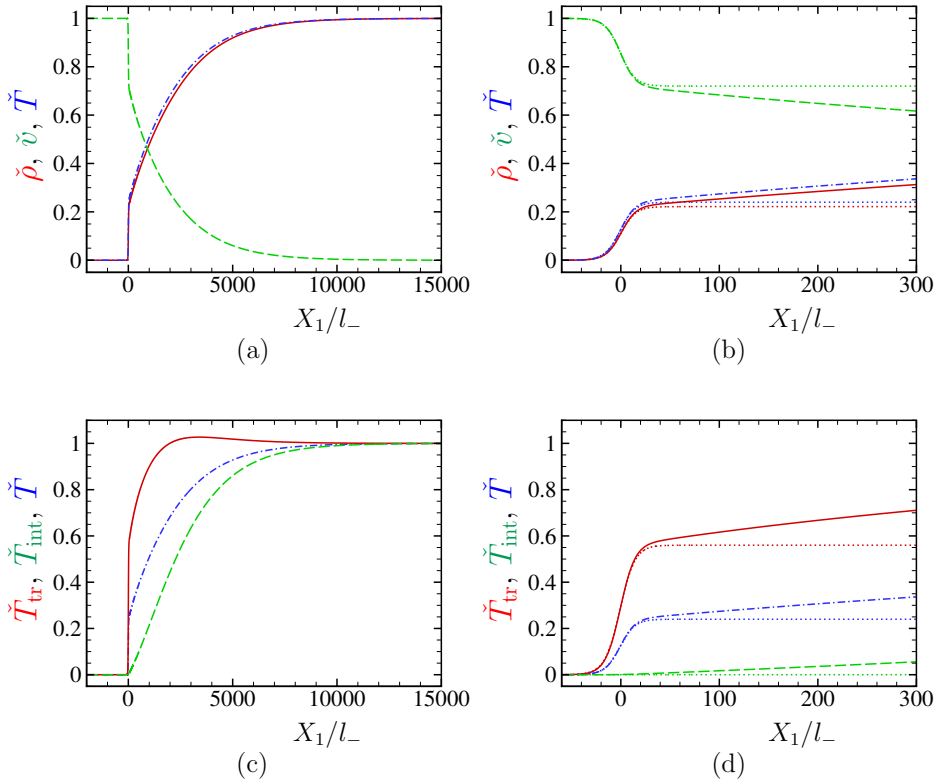

FIG. 3: Profiles of $\check{\rho}$, $\check{v}$, $\check{T}$, $\check{T}_{\rm tr}$, and $\check{T}_{\rm int}$ at $M_- = 1.2$ for $\mu_b/\mu = 1000$. (a) and (c) show profiles for $-2000 \le X_1/l_- \le 15000$; (b) and (d) those for $-30 \le X_1/l_- \le 300$. In (a) and (b), the red solid line indicates $\check{\rho}$, the green dashed line $\check{v}$, and the blue dot-dashed line $\check{T}$, and in (c) and (d), the red solid line indicates $\check{T}_{\rm tr}$, the green dashed line $\check{T}_{\rm int}$, and the blue dot-dashed line $\check{T}$. The dotted lines of the same color as the respective macroscopic quantities in (b) and (d) indicate the profiles obtained from Eq. (77) with $\theta = 0$ (i.e., $\mu_b/\mu = \infty$).

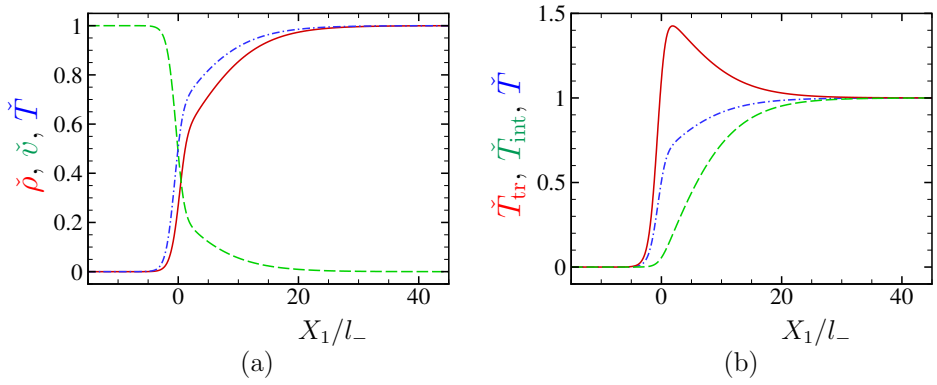

FIG. 4: Profiles $\check{\rho}$, $\check{v}$, $\check{T}$, $\check{T}_{\rm tr}$, and $\check{T}_{\rm int}$ at $M_- = 2$ for $\mu_b/\mu = 10$. See the caption of Fig. 1.

the present study, we also consider the pseudo-CO_2 gas with $\mu_b/\mu = 10$, 100, and 1000, which correspond to $\theta = 5.01\times10^{-2}$, 5.01×10^{-3}, and 5.01×10^{-4}, respectively [cf. Eq. (16)]. However, we will mainly show the result for $\mu_b/\mu = 1000$ in the present paper.

In the following, we show the profiles of the density ρ, the flow velocity v_1 (the X_1 component),

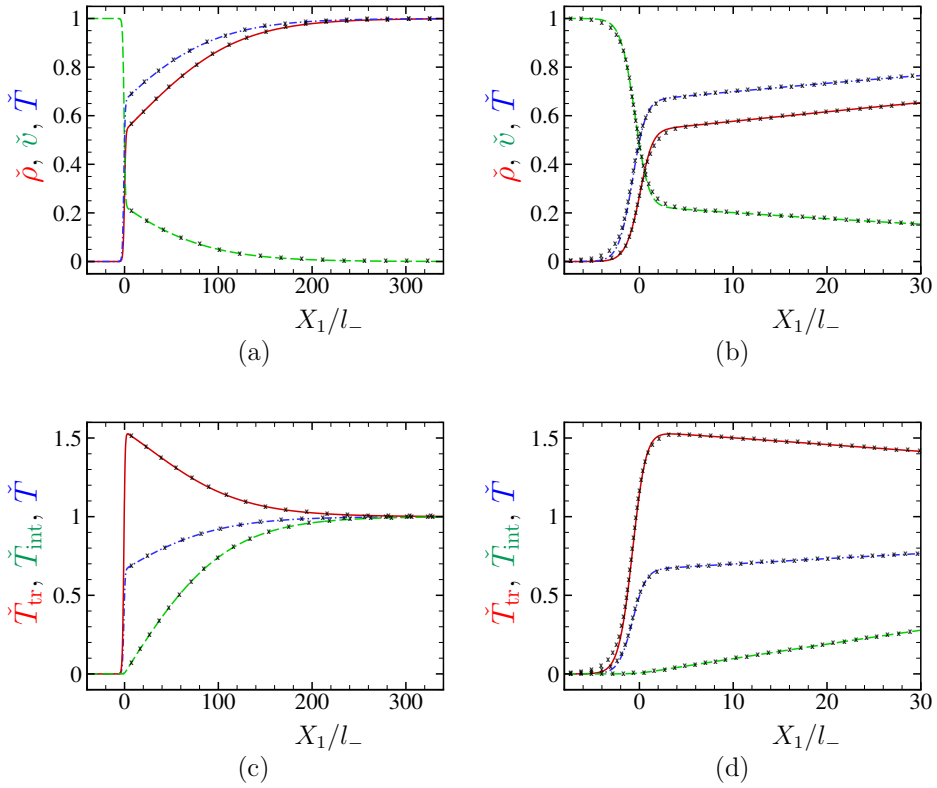

FIG. 5: Profiles of $\check{\rho}$, $\check{v}$, $\check{T}$, $\check{T}_{\rm tr}$, and $\check{T}_{\rm int}$ at $M_- = 2$ for $\mu_b/\mu = 100$. (a) and (c) show profiles for $-40 \le X_1/l_- \le 340$; (b) and (d) those for $-8 \le X_1/l_- \le 30$. See the caption of Fig. 3 for the types of the lines. The symbol $\times$ indicates the profiles based on the ES model.

and the temperatures T, $T_{\rm tr}$, and $T_{\rm int}$ normalized in the conventional way, that is,

$$\check{\rho} = \frac{\rho - \rho_-}{\rho_+ - \rho_-}, \qquad \check{v} = \frac{v_1 - v_+}{v_- - v_+}, \qquad \check{T} = \frac{T - T_-}{T_+ - T_-},$$
$$\check{T}_{\rm tr} = \frac{T_{\rm tr} - T_-}{T_+ - T_-}, \qquad \check{T}_{\rm int} = \frac{T_{\rm int} - T_-}{T_+ - T_-}. \tag{91}$$

We first show the profiles of the macroscopic quantities at $M_- = 1.05$ for $\mu_b/\mu = 1000$ in Fig. 1: Fig. 1(a) shows the profiles of $\check{\rho}$, $\check{v}$, and $\check{T}$, and Fig. 1(b) those of $\check{T}_{\rm tr}$, $\check{T}_{\rm int}$, and $\check{T}$. In Fig. 1(a), the red solid line indicates $\check{\rho}$, the green dashed line $\check{v}$, and the blue dot-dashed line $\check{T}$, and in Fig. 1(b), the red solid line indicates $\check{T}_{\rm tr}$, the green dashed line $\check{T}_{\rm int}$, and the blue dot-dashed line $\check{T}$. The origin $X_1 = 0$ is chosen in such a way that $\check{\rho} = 1/2$ at $X_1 = 0$. The curve of $\check{T}$ almost coincides with that of $\check{\rho}$. The profiles are smooth, but the shock wave is very thick and extends over 40000 mean free paths. This type of profiles, which is called Type A in [33–35], appears for M_- close to unity. For $\mu_b/\mu = 10$ and 100 (the results are not shown here), the profiles are similar, but the thickness becomes 1/100 and 1/10, respectively. The profiles obtained by the direct numerical analysis of the ES model in [31] agree perfectly with those in Fig. 1, so that the results are not shown in the figure.

Figure 2 shows the profiles of the macroscopic quantities at $M_- = 1.138$ for $\mu_b/\mu = 1000$: Fig. 2(a) shows the profiles of $\check{\rho}$, $\check{v}$, and $\check{T}$, and Fig. 2(b) those of $\check{T}_{\rm tr}$, $\check{T}_{\rm int}$, and $\check{T}$. The types of the lines are the same as those in Fig. 1. The origin $X_1 = 0$ is taken in such a way that $\check{\rho} = 0.05$ at $X_1 = 0$. The value $M_- = 1.138\ldots$ corresponds to the case of $\widetilde{M}_- = v_-/(5RT_-/3)^{1/2} = 1$, where $\widetilde{M}_-$ is the upstream Mach number when the gas is regarded as a monatomic gas. In contrast to Fig. 1, the profiles start suddenly, and each profile, except $\check{T}_{\rm int}$, exhibits a corner at the starting point. This type of profiles is called Type B in [33–35]. As was shown in [31], $\widetilde{M}_-$ plays an important role for the classification of the types of the profiles, and Type-A profiles appear for $\widetilde{M}_- < 1 < M_-$ and Type-B profiles for $1 = \widetilde{M}_- < M_-$. The profiles extend over

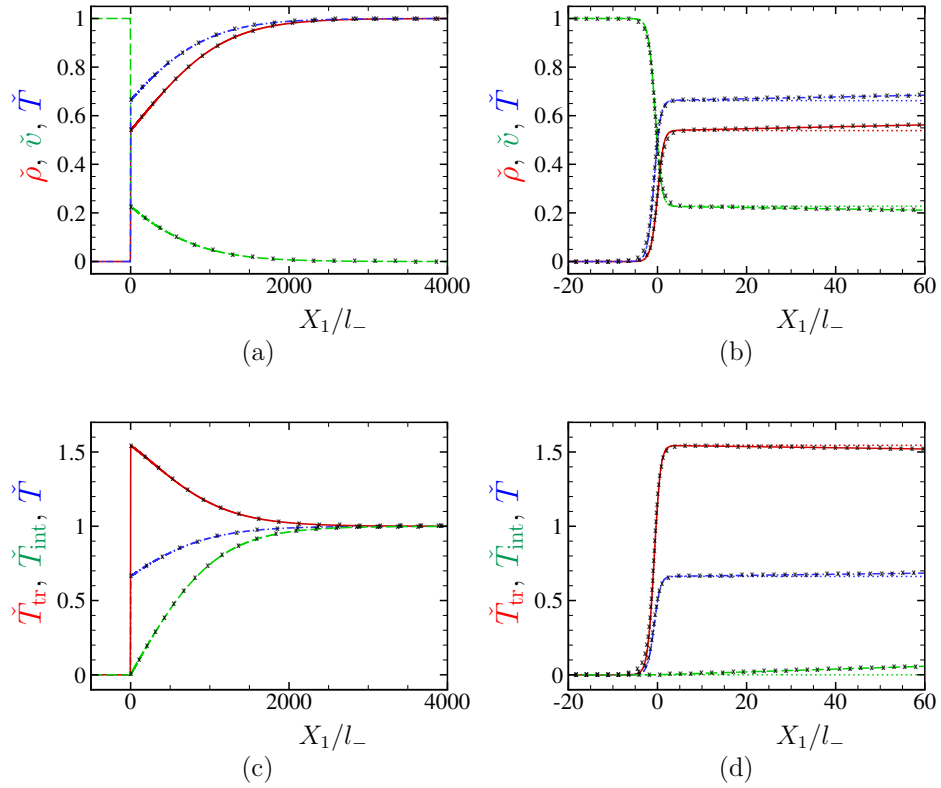

FIG. 6: Profiles of $\check{\rho}$, $\check{v}$, $\check{T}$, $\check{T}_{\rm tr}$, and $\check{T}_{\rm int}$ at $M_- = 2$ for $\mu_b/\mu = 1000$. (a) and (c) show profiles for $-500 \le X_1/l_- \le 4000$; (b) and (d) those for $-20 \le X_1/l_- \le 60$. See the caption of Fig. 3 for the types of the lines. The symbol $\times$ indicates the profiles based on the ES model.

15000 mean free paths. As μ_b/μ is smaller ($100 \to 10$) (the results are not shown here), the thickness reduces, and the start of the profiles becomes milder. Also in this case, the profiles based on the ES model are indistinguishable from those in Fig. 2, so that they are omitted in the figures.

In Fig. 3, we show the profiles at $M_- = 1.2$ for $\mu_b/\mu = 1000$: Figs. 3(a) and 3(b) show the profiles of $\check{\rho}$, $\check{v}$, and $\check{T}$, and Figs. 3(c) and 3(d) those of $\check{T}_{\rm tr}$, $\check{T}_{\rm int}$, and $\check{T}$. The types of the lines are the same as those in Fig. 1, and Figs. 3(b) and 3(d) are, respectively, the magnified figures of Figs. 3(a) and 3(c). In addition, the dotted lines of the same color as the respective macroscopic quantities in Figs. 3(b) and 3(d) indicate the profiles obtained from Eq. (77) with $\theta = 0$ (i.e., $\mu_b/\mu = \infty$). Each profile consists of a thin front layer with a sharp change, which looks like a discontinuity in Figs. 3(a) and 3(c), and a thick rear layer with a slow relaxation. This type of profiles is called Type C in [33–35]. The numerical analysis based on the ES model carried out in [31] shows that the thin front layer for small θ is nothing but the shock profile for $\theta = 0$, which satisfies the Rankine–Hugoniot relations different from Eq. (72) [see Eq. (A20) in [31]]. It is seen from Figs. 3(b) and 3(d) that this statement is also true in the level of the two-temperature Navier–Stokes equations. By the way, in Fig. 3 and Figs. 4–9 below, the origin $X_1 = 0$ is chosen in such a way that $\check{\rho} = \check{\rho}_*/2$ at $X_1 = 0$, where $\check{\rho}_*$ is the value of $\check{\rho}$ corresponding to the downstream density of the shock wave with $\theta = 0$. As in the previous cases, the profiles based on the ES model are not shown in the figure because they are indistinguishable from the profiles in Fig. 3.

Figures 4–6 show the profiles at $M_- = 2$ for $\mu_b/\mu = 10$, 100, and 1000, respectively. Figures 4(a), 5(a), 5(b), 6(a), and 6(b) show the profiles of $\check{\rho}$, $\check{v}$, and $\check{T}$, and Figs. 4(b), 5(c), 5(d), 6(c), and 6(d) those of $\check{T}_{\rm tr}$, $\check{T}_{\rm int}$, and $\check{T}$. The types of the lines are the same as those in Fig. 1, and Figs. 5(b), 5(d), 6(b), and 6(d) are, respectively, the magnified figures of Figs. 5(a), 5(c), 6(a), and 6(c). In addition, the dotted lines of the same color as the respective macroscopic quantities in Figs. 6(b) and 6(d) indicate the profiles obtained from Eq. (77) with $\theta = 0$ (i.e., $\mu_b/\mu = \infty$). These profiles are also of Type C. The changes across the thin front layer in Fig. 6

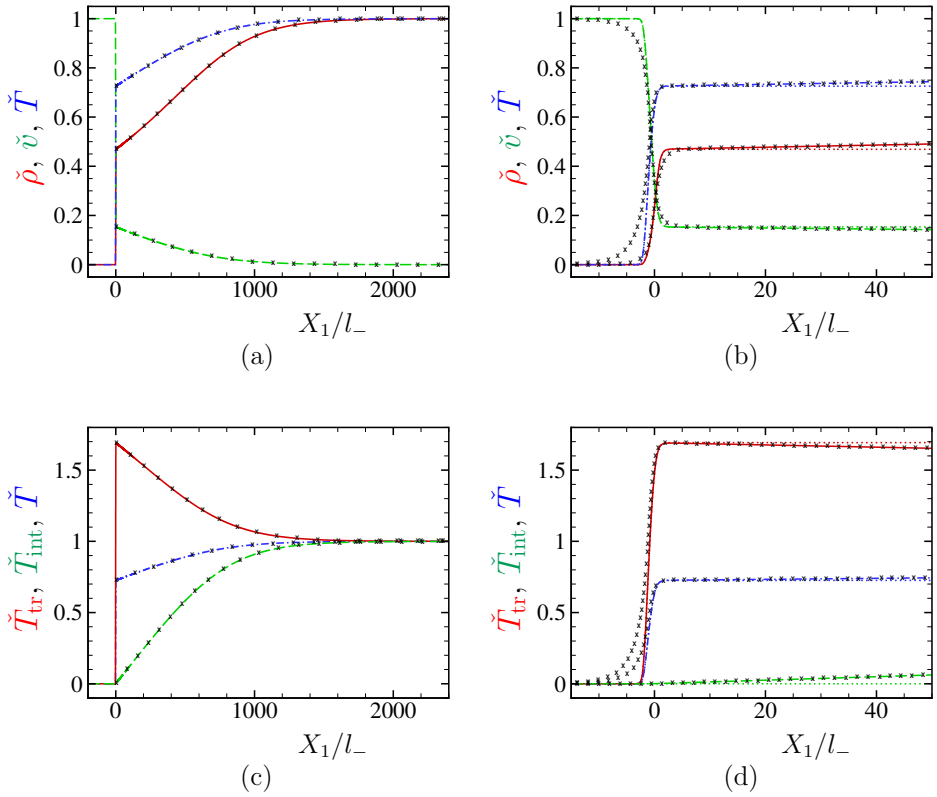

FIG. 7: Profiles of $\check{\rho}$, $\check{v}$, $\check{T}$, $\check{T}_{\rm tr}$, and $\check{T}_{\rm int}$ at $M_- = 5$ for $\mu_b/\mu = 1000$. (a) and (c) show profiles for $-200 \le X_1/l_- \le 2400$; (b) and (d) those for $-15 \le X_1/l_- \le 50$. See the caption of Fig. 3 for the types of the lines. The symbol $\times$ indicates the profiles based on the ES model.

is larger than those in Fig. 3. In Figs. 5(a)–5(d) and 6(a)–6(d), we show by $\times$ the profiles based on the ES model. Although there are small discrepancies between the profiles based on the two-temperature Navier–Stokes equations and those based on the ES model at the onset of the thin front layer, the agreement is very good on the whole.

In Fig. 7, the profiles at $M_- = 5$ for $\mu_b/\mu = 1000$ are shown: Figs. 7(a) and 7(b) show the profiles of $\check{\rho}$, $\check{v}$, and $\check{T}$, and Figs. 7(c) and 7(d) those of $\check{T}_{\rm tr}$, $\check{T}_{\rm int}$, and $\check{T}$. The types of the lines are the same as those in Fig. 1, and Figs. 7(b) and 7(d) are, respectively, the magnified figures of Figs. 7(a) and 7(c). In addition, the dotted lines of the same color as the respective macroscopic quantities in Figs. 7(b) and 7(d) indicate the profiles obtained from Eq. (77) with $\theta = 0$ (i.e., $\mu_b/\mu = \infty$). Although the thickness of the rear layer is reduced compared with Fig. 6, it still extends over 2000 mean free paths. In Figs. 7(a)–7(d), the profiles based on the ES model are also shown by $\times$. There is a significant difference between the profiles based on the two-temperature Navier–Stokes equations and those based on the ES model in the thin front layer. The ES model gives a milder and thicker front layer. Nevertheless, both results agree very well in the thick rear layer.

Finally in Figs. 8 and 9, we show the profiles at $M_- = 2$ for $\mu_b/\mu = 1000$ in the case of different values of the number of the internal degrees of freedom δ, that is, Fig. 8 is for $\delta = 3$, and Fig. 9 for $\delta = 5$. The figures correspond to Fig. 6, so that we omit the explanation of the figures. Since the agreement between the profiles based on the two-temperature Navier–Stokes equations and those based on the ES model is in the same level as in Fig. 6, we omit the latter in the figures.

In summary, the system of the two-temperature Navier–Stokes equations describes the shock wave structure for CO_2 gas very well when the upstream Mach number is less than or equal to 2. In this case, it describes even the structure of the thin front layer in Type-C profiles correctly. For $M_- = 5$, however, it looses the accuracy in describing the structure of the thin front layer. Nevertheless, it still describes the thick rear layer with a slow relaxation very well.

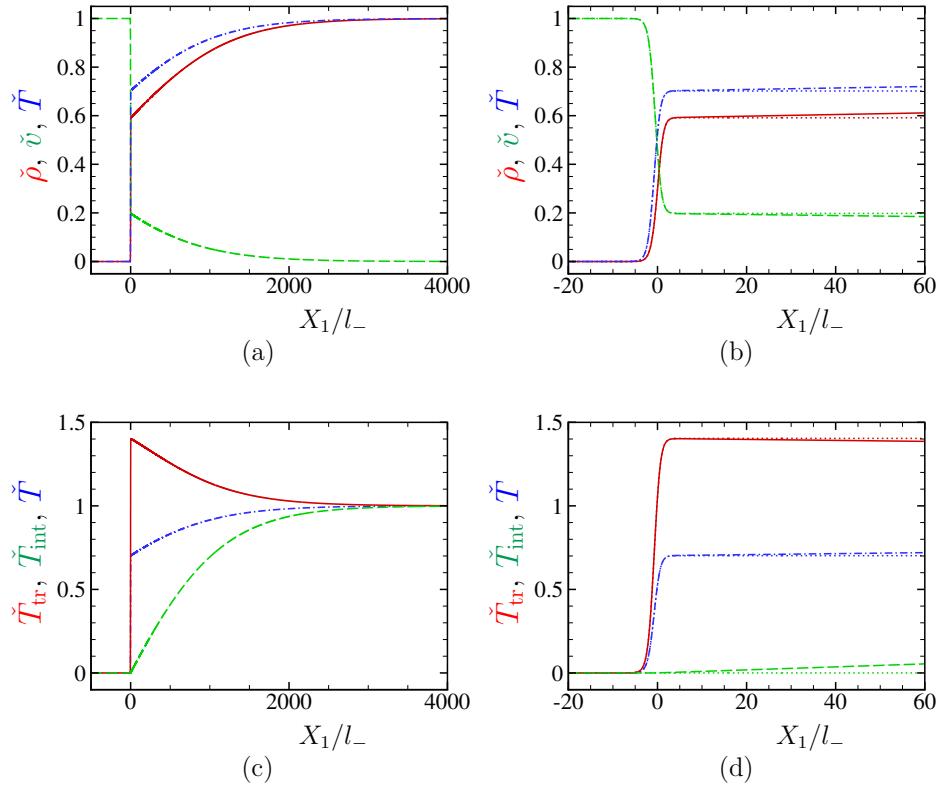

FIG. 8: Profiles of $\check{\rho}$, $\check{v}$, $\check{T}$, $\check{T}_{\rm tr}$, and $\check{T}_{\rm int}$ at $M_- = 2$ for $\mu_b/\mu = 1000$ in the case of $\delta = 3$. (a) and (c) show profiles for $-500 \le X_1/l_- \le 4000$; (b) and (d) those for $-20 \le X_1/l_- \le 60$. See the caption of Fig. 3 for the types of the lines.

The data of the numerical analysis are summarized in Appendix B.

V. CONCLUDING REMARKS

The present study is devoted to the derivation of the two-temperature Navier–Stokes equations, i.e., a system of Navier–Stokes type equations with two temperatures, one associated with the translational energy and the other associated with the energy of the internal modes, for a polyatomic gas with slow relaxation of the internal modes. The starting point is the ES model of the Boltzmann equation for a polyatomic gas, and the desired two-temperature Navier–Stokes system was obtained by the Chapman–Enskog expansion with an appropriate setting of small parameters.

The ES model is a simple and overall model that, as well as other BGK-type models, does not contain detailed information about molecular structures, such as the atomic and molecular potentials. However, BGK-type models are often used for practical applications, since the Boltzmann equation with such detailed information, which depends on individual gases and is not necessarily available, is extremely complicated and its use is quite limited. The two-temperature Navier–Stokes system derived here inherits the simplicity and the overall nature of the ES model. Therefore, one should not expect that the system describes the properties that directly depend on the detailed molecular structure. On the other hand, the parameters contained in the system are determined only by the overall properties of gases, such as the viscosity and the bulk viscosity, and can, in principle, be estimated experimentally. Therefore, it can be applied to practical flow problems for a wide range of polyatomic gases without the knowledge of the detailed molecular structures.

In fact, the derived system was applied to the problem of the structure of a plane shock wave in CO_2 gas, and its numerical solution showed good agreement with that of the ES model for a moderately strong shock wave ($M_- = 2$). Even for a stronger shock wave ($M_- = 5$),

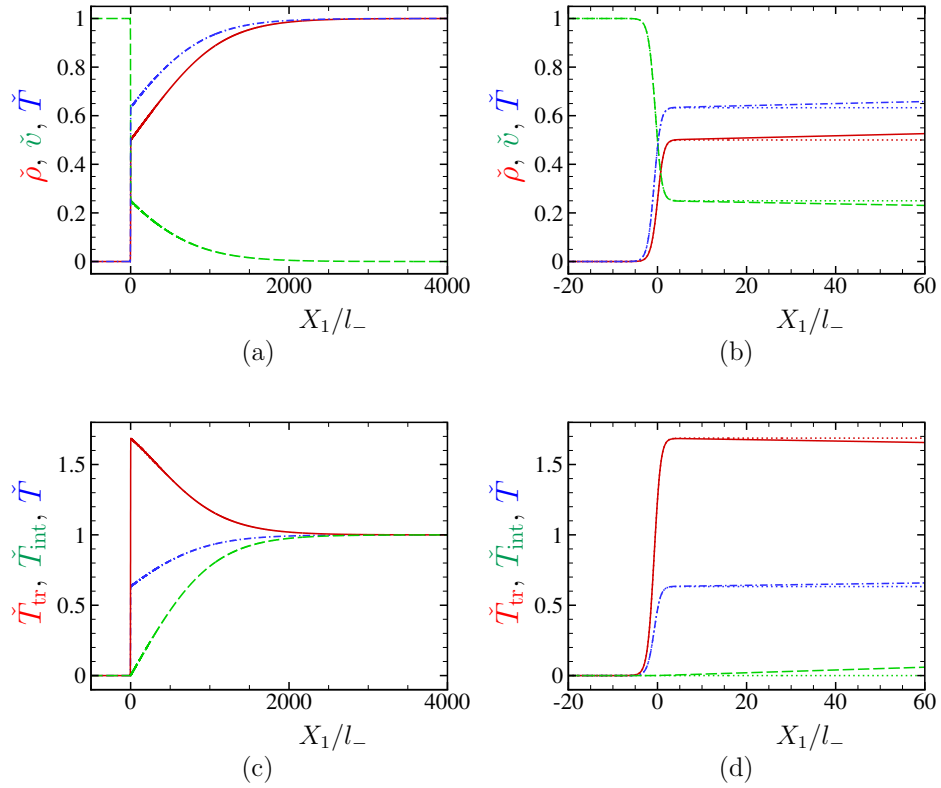

FIG. 9: Profiles of $\check{\rho}$, $\check{v}$, $\check{T}$, $\check{T}_{\rm tr}$, and $\check{T}_{\rm int}$ at $M_- = 2$ for $\mu_b/\mu = 1000$ in the case of $\delta = 5$. (a) and (c) show profiles for $-500 \le X_1/l_- \le 4000$; (b) and (d) those for $-20 \le X_1/l_- \le 60$. See the caption of Fig. 3 for the types of the lines.

although not accurate inside the thin front shock layer, the numerical solution of the two-temperature Navier–Stokes system describes the thick rear shock layer accurately. This is one of the promising features of the system for highly nonequilibrium flows of a gas with slow relaxation of the internal modes. We plan to investigate, in our future work, the behavior of the steady shock wave solution of the two-temperature Navier–Stokes system for higher Mach numbers, including the stability properties of the equilibrium states (cf. the last paragraph in Sec. IV C).

The present study is based on the ES model for a gas with constant specific heats (calorically perfect gas). The ES model has been extended to a gas with temperature-dependent specific heats (thermally perfect gas) in a recent paper [18]. If we use this extended ES model, the two-temperature Navier–Stokes equations are readily extended to a thermally perfect gas.

Another advantage of the present system of two-temperature Navier–Stokes equations compared with higher-order moment equations (e.g., [33]) is that it is straightforward to derive the appropriate slip boundary conditions on the solid boundary by following the procedure in [41, 59]. This would be a subject of a future study.

Acknowledgments

The present study was initiated while K.A. was visiting the Department of Mathematical, Physical and Computer Sciences, University of Parma as Visiting Professor. He wishes to thank the Department for the invitation and the kind hospitality. His thanks are also due to Professor Giampiero Spiga for his kind hospitality and support. The authors M.B. and M.G. thank the support by the University of Parma, by the Italian National Group of Mathematical Physics (GNFM-INdAM), and by the Italian National Research Project *Multiscale phenomena in Continuum Mechanics: singular limits, off-equilibrium and transitions* (Prin 2017YBKNCE). The authors thank Professors Vincent Giovangigli, Elena Kustova, and Masaru Sugiyama for

their interest and valuable comments.

Appendix A: Expansion of $\hat{\mathcal{G}}$

In this Appendix, we calculate the terms $\hat{\mathcal{G}}^{(0)}$ and $\hat{\mathcal{G}}^{(1)}$ in the expansion (56) of $\hat{\mathcal{G}}$ [cf. Eq. (25b)]. Here, let us recall Eq. (33), i.e.,

$$\theta = \alpha\epsilon \ll 1. \tag{A1}$$

The leading-order term is $\hat{\mathcal{G}}^{(0)} = \hat{\mathcal{G}}|_{\epsilon=0} = \hat{\mathcal{G}}|_{\theta=0}$, and as mentioned in Sec. III B 2, $\hat{f}^{(0)}$ solves the equation $\hat{\mathcal{G}}^{(0)} - \hat{f}^{(0)} = 0$. Therefore,

$$\hat{\mathcal{G}}^{(0)} = \hat{f}^{(0)} = \frac{\hat{\rho}\,\hat{\mathcal{E}}^{\delta/2-1}}{(\pi\hat{T}_{\rm tr})^{3/2}\hat{T}_{\rm int}^{\delta/2}\Gamma(\delta/2)} \exp\left(-\frac{|\boldsymbol{\zeta}-\hat{\boldsymbol{v}}|^2}{\hat{T}_{\rm tr}} - \frac{\hat{\mathcal{E}}}{\hat{T}_{\rm int}}\right). \tag{A2}$$

The first-order term $\hat{\mathcal{G}}^{(1)}$ is calculated as follows. The quantities that depend on ϵ in $\hat{\mathcal{G}}$ when $\theta = \alpha\epsilon$ are only $\hat{T}_{\rm rel}$ and the 3×3 matrix $\hat{\mathsf{T}}$. We have already expanded $\hat{T}_{\rm rel}$ and $\hat{p}_{ij}$, which is contained in $\hat{\mathsf{T}}$, in Eq. (43). In addition, we need to expand $\hat{\mathsf{T}}$, $\hat{\mathsf{T}}^{-1}$, and $\det\hat{\mathsf{T}}$, that is,

$$H = H^{(0)} + H^{(1)}\epsilon + \cdots, \qquad (H = \hat{\mathsf{T}},\ \hat{\mathsf{T}}^{-1},\ \text{and}\ \det\hat{\mathsf{T}}). \tag{A3}$$

It follows directly from Eqs. (25c) and (50) that

$$(\hat{\mathsf{T}}^{(0)})_{ij} = (1-\nu)\hat{T}_{\rm tr}\delta_{ij} + \frac{\nu}{\hat{\rho}}\hat{p}_{ij}^{(0)} = \hat{T}_{\rm tr}\delta_{ij}, \tag{A4a}$$

$$(\hat{\mathsf{T}}^{(1)})_{ij} = \alpha[\hat{T} - (1-\nu)\hat{T}_{\rm tr}]\delta_{ij} + \frac{\nu}{\hat{\rho}}(\hat{p}_{ij}^{(1)} - \alpha\hat{p}_{ij}^{(0)}) = \frac{\nu}{\hat{\rho}}\hat{p}_{ij}^{(1)} + \alpha(\hat{T}-\hat{T}_{\rm tr})\delta_{ij}, \tag{A4b}$$

$$\cdots.$$

Noting that $\hat{\mathsf{T}}\hat{\mathsf{T}}^{-1} = (\hat{\mathsf{T}}^{(0)} + \hat{\mathsf{T}}^{(1)}\epsilon + \cdots)[(\hat{\mathsf{T}}^{-1})^{(0)} + (\hat{\mathsf{T}}^{-1})^{(1)}\epsilon + \cdots] = \mathsf{I}$, where I is the 3×3 unit matrix, we have $(\hat{\mathsf{T}}^{-1})^{(0)} = (\hat{\mathsf{T}}^{(0)})^{-1}$, $(\hat{\mathsf{T}}^{-1})^{(1)} = -(\hat{\mathsf{T}}^{(0)})^{-1}\hat{\mathsf{T}}^{(1)}(\hat{\mathsf{T}}^{-1})^{(0)}$, etc. This means that

$$(\hat{\mathsf{T}}^{-1})_{ij}^{(0)} = \frac{1}{\hat{T}_{\rm tr}}\delta_{ij}, \qquad (\hat{\mathsf{T}}^{-1})_{ij}^{(1)} = -\frac{1}{\hat{T}_{\rm tr}^2}\left[\frac{\nu}{\hat{\rho}}\hat{p}_{ij}^{(1)} + \alpha(\hat{T}-\hat{T}_{\rm tr})\delta_{ij}\right], \quad \cdots. \tag{A5}$$

In addition, let us note that $(\det\hat{\mathsf{T}})^{(0)} = (\det\hat{\mathsf{T}})_{\epsilon=0} = \det(\hat{\mathsf{T}}^{(0)})$, $(\det\hat{\mathsf{T}})^{(1)} = [d(\det\hat{\mathsf{T}})/d\epsilon]_{\epsilon=0}$, etc. Therefore, we obtain the following:

$$(\det\hat{\mathsf{T}})^{(0)} = \hat{T}_{\rm tr}^3, \tag{A6a}$$

$$\begin{aligned}(\det\hat{\mathsf{T}})^{(1)} &= \det\begin{bmatrix}(\hat{\mathsf{T}}^{(1)})_{11} & (\hat{\mathsf{T}}^{(0)})_{12} & (\hat{\mathsf{T}}^{(0)})_{13}\\ (\hat{\mathsf{T}}^{(1)})_{21} & (\hat{\mathsf{T}}^{(0)})_{22} & (\hat{\mathsf{T}}^{(0)})_{23}\\ (\hat{\mathsf{T}}^{(1)})_{31} & (\hat{\mathsf{T}}^{(0)})_{32} & (\hat{\mathsf{T}}^{(0)})_{33}\end{bmatrix} + \det\begin{bmatrix}(\hat{\mathsf{T}}^{(0)})_{11} & (\hat{\mathsf{T}}^{(1)})_{12} & (\hat{\mathsf{T}}^{(0)})_{13}\\ (\hat{\mathsf{T}}^{(0)})_{21} & (\hat{\mathsf{T}}^{(1)})_{22} & (\hat{\mathsf{T}}^{(0)})_{23}\\ (\hat{\mathsf{T}}^{(0)})_{31} & (\hat{\mathsf{T}}^{(1)})_{32} & (\hat{\mathsf{T}}^{(0)})_{33}\end{bmatrix}\\ &\quad + \det\begin{bmatrix}(\hat{\mathsf{T}}^{(0)})_{11} & (\hat{\mathsf{T}}^{(0)})_{12} & (\hat{\mathsf{T}}^{(1)})_{13}\\ (\hat{\mathsf{T}}^{(0)})_{21} & (\hat{\mathsf{T}}^{(0)})_{22} & (\hat{\mathsf{T}}^{(1)})_{23}\\ (\hat{\mathsf{T}}^{(0)})_{31} & (\hat{\mathsf{T}}^{(0)})_{32} & (\hat{\mathsf{T}}^{(1)})_{33}\end{bmatrix}\\ &= \left[\frac{\nu}{\hat{\rho}}\,\hat{p}_{kk}^{(1)} + 3\alpha(\hat{T}-\hat{T}_{\rm tr})\right]\hat{T}_{\rm tr}^2,\end{aligned} \tag{A6b}$$

$$\cdots.$$

It follows from Eq. (57) that $\hat{\mathcal{G}}^{(1)} = [\hat{\mathcal{G}}(d\log\hat{\mathcal{G}}/d\epsilon)]_{\epsilon=0} = \hat{\mathcal{G}}^{(0)}[d\log\hat{\mathcal{G}}/d\epsilon]_{\epsilon=0} =$

$\hat{f}^{(0)}[d\log\hat{\mathcal{G}}/d\epsilon]_{\epsilon=0}$. Therefore, using Eq. (25b), we have

$$\begin{aligned}\frac{1}{\hat{f}^{(0)}}\hat{\mathcal{G}}^{(1)} &= -\frac{1}{2}\frac{(\det\hat{\mathsf{T}})^{(1)}}{(\det\hat{\mathsf{T}})^{(0)}} + \left(\frac{\hat{\mathcal{E}}}{\hat{T}_{\rm rel}^{(0)}} - \frac{\delta}{2}\right)\frac{\hat{T}_{\rm rel}^{(1)}}{\hat{T}_{\rm rel}^{(0)}} - (\zeta_i - \hat{v}_i)(\zeta_j - \hat{v}_j)(\hat{\mathsf{T}}^{-1})_{ij}^{(0)} \\ &= \nu\left[\frac{(\zeta_i - \hat{v}_i)(\zeta_j - \hat{v}_j)}{\hat{T}_{\rm tr}} - \frac{1}{2}\delta_{ij}\right]\frac{\hat{p}_{ij}^{(1)}}{\hat{\rho}\hat{T}_{\rm tr}} + \alpha\left[\frac{(\zeta_k - \hat{v}_k)^2}{\hat{T}_{\rm tr}} - \frac{3}{2}\right]\frac{\hat{T} - \hat{T}_{\rm tr}}{\hat{T}_{\rm tr}} \\ &\quad + \alpha\left(\frac{\hat{\mathcal{E}}}{\hat{T}_{\rm int}} - \frac{\delta}{2}\right)\frac{\hat{T} - \hat{T}_{\rm int}}{\hat{T}_{\rm int}}. \end{aligned} \tag{A7}$$

This gives Eq. (58).

Appendix B: Data for numerical analysis

The length of the grid interval $\Delta\eta_i$ is either uniform or variable. In the latter case, the grid point η_i is defined by using Eq. (B1) in Appendix B of [31]. To be more specific, $\eta_i = (2/\sqrt{\pi})x_{(i)} = 1.128x_{(i)}$, where $x_{(i)}$ is given by Eq. (B1) in [31] with $a = p = 3$, $b = 1$, and $q = 2$. The other parameters and the time step Δt are shown in Table I. Starting from the initial condition, we consider the steady state to have been established when the following condition is satisfied:

$$\max_{-N_n<i<N_p} |h_i^n - h_i^{n-1}| < \sigma = 10^{-10}, \qquad (h = \rho,\, v,\, T_{\rm tr}, \text{ and } T_{\rm int}), \tag{B1}$$

where and in Eq. (B2) below, the change of notation (81) is used. As a measure of accuracy of the computation, we also show, in Table I, the value of

$$d = \max_{-N_n<i<N_p} |(\rho_i^n v_i^n - \hat{v}_-)/\hat{v}_-|, \tag{B2}$$

which should be zero theoretically.

[1] J. H. Ferziger and H. G. Kaper, *Mathematical Theory of Transport Processes in Gases* (North Holland, Amsterdam, 1972).

[2] F. R. W. McCourt, J. J. M. Beenakker, W. E. Köhler, and I. Kuščer, *Nonequilibrium Phenomena in Polyatomic Gases, Volume 1: Dilute Gases* (Clarendon, Oxford, 1990).

[3] A. Rossani and G. Spiga, Kinetic theory with inelastic interactions, Transp. Theor. Stat. Phys. **27**, 273–287 (1998).

[4] V. Giovangigli, *Multicomponent Flow Modeling* (Birkhäuser, Boston, 1999).

[5] L. Desvillettes, R. Monaco, and F. Salvarani, A kinetic model allowing to obtain the energy law of polytropic gases in the presence of chemical reactions, Eur. J. Mech. B/Fluids **24**, 219–236 (2005).

[6] E. Nagnibeda and E. Kustova, *Non-Equilibrium Reacting Gas Flows: Kinetic Theory of Transport and Relaxation Processes* (Springer, Berlin, 2009).

[7] G. M. Kremer, *An Introduction to the Boltzmann Equation and Transport Processes in Gases* (Springer, Berlin, 2010).

[8] T. F. Morse, Kinetic model for gases with internal degrees of freedom, Phys. Fluids **7**, 159–169 (1964).

[9] L. H. Holway, Jr., New statistical models for kinetic theory: Methods of construction, Phys. Fluids **9**, 1658–1673 (1966).

[10] V. A. Rykov, A model kinetic equation for a gas with rotational degrees of freedom, Fluid Dyn. **10**, No. 6, 959–966 (1975).

[11] M. Groppi and G. Spiga, Kinetic approach to chemical reactions and inelastic transitions in a rarefied gas, J. Math. Chem. **26**, 197–219 (1999).

[12] H. Struchtrup, The BGK model for an ideal gas with an internal degree of freedom, Transp. Theor. Stat. Phys. **28**, 369–385 (1999).

[13] P. Andries, P. Le Tallec, J.-P. Perlat, and B. Perthame, The Gaussian-BGK model of Boltzmann equation with small Prandtl number, Eur. J. Mech. B/Fluids **19**, 813–830 (2000).

TABLE I: Data for numerical computation.

M_-	μ_b/μ	D_n, N_n	D_p, N_p	$\Delta\eta_i$	Δt	d
1.05	10	1128, 2000	1128, 2000	0.564[a]	0.0282	7.6(−7)[b]
	100	11284, 2000	11284, 2000	5.64[a]	0.226	5.8(−7)
	1000	56419, 2000	56419, 2000	28.2[a]	0.564	2.8(−6)
1.138	10	564, 2000	564, 2000	0.282[a]	7.05(−3)	6.8(−7)
	100	564, 500	5642, 1400	0.282–8.46	7.05(−3)	4.6(−6)
	1000	9027, 800	45135, 1440	2.82–84.6	0.113	3.2(−6)
1.2	10	451, 2000	451, 2000	0.226[a]	4.51(−3)	7.0(−7)
	100	564, 500	3385, 1000	0.282–8.46	7.05(−3)	1.0(−6)
	1000	2708, 1200	33851, 3960	0.564–16.9	0.0282	3.7(−7)
2	10	56.4, 1000	113, 2000	0.0564[a]	2.82(−4)	1.2(−6)
	100	226, 800	1128, 1440	0.0705–2.11	4.51(−4)	1.2(−6)
	1000	564, 2000	11284, 9600	0.0705–2.11	4.51(−4)	1.0(−5)[c]
5	10	56.4, 1000	90.3, 1600	0.0564[a]	2.82(−4)	3.8(−6)
	100	113, 500	564, 900	0.0564–1.69	2.82(−4)	2.9(−6)
	1000	226, 1000	5642, 5800	0.0564–1.69	2.82(−4)	3.0(−6)

[a]Uniform grid.
[b]Read as 7.6×10^{-7}.
[c]$\sigma = 2.4 \times 10^{-10}$ in Eq. (B1).

[14] B. Rahimi and H. Struchtrup, Macroscopic and kinetic modelling of rarefied polyatomic gases, J. Fluid Mech. **806**, 437–505 (2016).
[15] M. Bisi and G. Spiga, On kinetic models for polyatomic gases and their hydrodynamic limits, Ricerche Mat. **66**, 113–124 (2017).
[16] M. Bisi, T. Ruggeri, and G. Spiga, Dynamical pressure in a polyatomic gas: Interplay between kinetic theory and extended thermodynamics, Kinet. Relat. Mod. **11**, 71–95 (2018).
[17] T. Arima, T. Ruggeri, and M. Sugiyama, Extended thermodynamics of rarefied polyatomic gases: 15-field theory incorporating relaxation processes of molecular rotation and vibration, Entropy **20**, 301 (2018).
[18] S. Kosuge, H.-W. Kuo, and K. Aoki, A kinetic model for a polyatomic gas with temperature-dependent specific heats and its application to shock-wave structure, J. Stat. Phys. **177**, 209–251 (2019).
[19] C. Baranger, Y. Dauvois, G. Marois, J. Mathé, J. Mathiaud, and L. Mieussens, A BGK model for high temperature rarefied gas flows, Eur. J. Mech. B/Fluids **80**, 1–12 (2020).
[20] D. Bruno and V. Giovangigli, Relaxation of internal temperature and volume viscosity, Phys. Fluids **23**, 093104 (2011); Erratum, Phys. Fluids **25**, 039902 (2013).
[21] T. Arima, S. Taniguchi, T. Ruggeri, and M. Sugiyama, Extended thermodynamics of real gases with dynamic pressure: an extension of Meixner's theory, Phys. Lett. A **376**, 2799–2803 (2012).
[22] T. Arima, T. Ruggeri, M. Sugiyama, and S. Taniguchi, Non-linear extended thermodynamics of real gases with 6 fields, Int. J. Non-Linear Mech. **72**, 6–15 (2015).
[23] T. Ruggeri and M. Sugiyama, *Rational Extended Thermodynamics beyond the Monatomic Gas* (Springer International Publishing Switzerland, 2015).
[24] T. Ruggeri, Non-linear maximum entropy principle for a polyatomic gas subject to the dynamic pressure, Bulletin of the Institute of Mathematics, Academia Sinica (New Series), **11**, 1–22 (2016).
[25] E. Kustova, M. Mekhonoshina, and A. Kosareva, Relaxation processes in carbon dioxide, Phys. Fluids **31**, 046104 (2019).
[26] M. Bisi and M. J. Cáceres, A BGK relaxation model for polyatomic gas mixtures, Commun. Math. Sci. **14**, 297–325 (2016).
[27] M. Bisi, R. Monaco, and A. J. Soares, A BGK model for reactive mixtures of polyatomic gases with continuous internal energy, J. Phys. A - Math. Theor. **51**, 125501 (2018).
[28] S. Chapman and T. G. Cowling, *The Mathematical Theory of Non-uniform Gases*, 3rd edition

(Cambridge Univ. Press, Cambridge, 1991).
[29] S. Brull and J. Schneider, On the ellipsoidal statistical model for polyatomic gases, Continuum Mech. Thermodyn. **20**, 489–508 (2009).
[30] S. Kosuge, K. Aoki, and T. Goto, Shock wave structure in polyatomic gases: Numerical analysis using a model Boltzmann equation, in *30th International Symposium on Rarefied Gas Dynamics: AIP Conf. Proc. 1786*, edited by A. Ketsdever and H. Struchtrup (AIP, Melville, 2016), 180004.
[31] S. Kosuge and K. Aoki, Shock-wave structure for a polyatomic gas with large bulk viscosity, Phys. Rev. Fluids **3**, 023401 (2018).
[32] S. Taniguchi, T. Arima, T. Ruggeri, and M. Sugiyama, Effect of the dynamic pressure on the shock wave structure in a rarefied polyatomic gas, Phys. Fluids **26**, 016103 (2014).
[33] S. Taniguchi, T. Arima, T. Ruggeri, and M. Sugiyama, Thermodynamic theory of the shock wave structure in a rarefied polyatomic gas: Beyond the Bethe-Teller theory, Phys. Rev. E **89**, 013025 (2014).
[34] S. Taniguchi, T. Arima, T. Ruggeri, and M. Sugiyama, Overshoot of the non-equilibrium temperature in the shock wave structure of a rarefied polyatomic gas subject to the dynamic pressure, Int. J. Non-Linear Mech. **79**, 66–75 (2016).
[35] S. Taniguchi, T. Arima, T. Ruggeri, and M. Sugiyama, Shock wave structure in rarefied polyatomic gases with large relaxation time for the dynamic pressure, IOP Conf. Series: J. Phys.: Conf. Series **1035**, 012009 (2018).
[36] G. A. Bird, *Molecular Gas Dynamics and the Direct Simulation of Gas Flows* (Oxford University Press, Oxford, 1994).
[37] C. Borgnakke and P. S. Larsen, Statistical collision model for Monte Carlo simulation of polyatomic gas mixture, J. Comp. Phys. **18**, 405–420 (1975).
[38] T. Tokumasu and Y. Matsumoto, Dynamic molecular collision (DMC) model for rarefied gas flow simulations by the DSMC method, Phys. Fluids **11**, 1907–1920 (1999).
[39] S. Takata, H. Funagane, and K. Aoki, Fluid modeling for the Knudsen compressor: Case of polyatomic gases, Kinet. Relat. Mod. **3**, 353–372 (2010).
[40] H. Funagane, S. Takata, K. Aoki, and K. Kugimoto, Poiseuille flow and thermal transpiration of a rarefied polyatomic gas through a circular tube with applications to microflows, Bollettino dell'Unione Matematica Italiana Ser. 9, **4**, 19–46 (2011).
[41] M. Hattori, S. Kosuge, and K. Aoki, Slip boundary conditions for the compressible Navier–Stokes equations for a polyatomic gas, Phys. Rev. Fluids **3**, 063401 (2018).
[42] P. A. Thompson, *Compressible-Fluid Dynamics* (McGraw-Hill, New York, 1972).
[43] G. Emanuel, Bulk viscosity of a dilute polyatomic gas, Phys. Fluids A **2**, 2252–2254 (1990).
[44] M. S. Cramer, Numerical estimates for the bulk viscosity of ideal gases, Phys. Fluids **24**, 066102 (2012).
[45] G. Billet, V. Giovangigli, and G. de Gassowski, Impact of volume viscosity on a shock-hydrogen-bubble interaction, Combust. Theory Model **12**, 221–248 (2008).
[46] W. E. Meador, G. A. Miner, and L. W. Townsend, Bulk viscosity as a relaxation parameter: Fact or fiction?, Phys. Fluids **8**, 258–261 (1996).
[47] M. N. Kogan, *Rarefied Gas Dynamics* (Plenum, New York, 1969).
[48] C. Cercignani, *The Boltzmann Equation and Its Applications* (Springer, Berlin, 1988).
[49] C. Cercignani, *Rarefied Gas Dynamics: From Basic Concepts to Actual Calculations* (Cambridge Univ. Press, Cambridge, 2000).
[50] Y. Sone, *Molecular Gas Dynamics: Theory, Techniques, and Applications* (Birkhäuser, Boston, 2007).
[51] I. Müller and T. Ruggeri, *Rational Extended Thermodynamics* (Springer, New York, 1998).
[52] H. Struchtrup, *Macroscopic Transport Equations for Rarefied Gas Flows* (Springer, Berlin, 2005).
[53] M. Pavić-Čolić, D. Madjarević, and S. Simić, Polyatomic gases with dynamic pressure: Kinetic non-linear closure and the shock structure, Int. J. Non-Linear Mech. **92**, 160–175 (2017).
[54] N. Hirose, M. Ikegawa, N. Tosaka, H. Kubota, and H. Honma, *Analysis of Compressible Flows*, Computational Fluid Dynamics Series 2, edited by N. Tosaka (University of Tokyo Press, Tokyo, 1995) (in Japanese).
[55] J. D. Anderson, Jr., *Hypersonic and High Temperature Gas Dynamics, 2nd ed.* (AIAA, Reston, 2006).
[56] T. G. Elizarova, A. A. Khokhlov, and S. Montero, Numerical simulation of shock wave structure in nitrogen, Phys. Fluids **19**, 068102 (2007).
[57] I. V. Alekseev, A. A. Kosareva, E. V. Kustova, and E. A. Nagnibeda, Various continuum approaches for studying shock wave structure in carbon dioxide, in *8th Polyakhov's Reading: AIP Conf. Proc. 1959*, edited by E. Kustova, G. Leonov, N. Morosov, M. Yushkov, and M. Mekhonoshina (AIP, Melville, 2018), 060001.
[58] I. V. Alekseev, A. A. Kosareva, E. V. Kustova, and E. A. Nagnibeda, Shock waves in carbon dioxide: Simulations using different kinetic-theory models, in *31st International Symposium on Rarefied Gas Dynamics: AIP Conf. Proc. 2132*, edited by Y. Zhang, D. R. Emerson, D. Lockerby,

and L. Wu (AIP, Melville, 2019), 060005.
[59] K. Aoki, C. Baranger, M. Hattori, S. Kosuge, G. Martalò, J. Mathiaud, and L. Mieussens, Slip boundary conditions for the compressible Navier–Stokes equations, J. Stat. Phys. **169**, 744–781 (2017).